THE GEOLOGICAL SOCIETY OF AMERICA®

Analysis of Elevation Changes Detected from Multi-Temporal LiDAR Surveys in Forested Landslide Terrain in Western Oregon

WILLIAM J. BURNS

Oregon Department of Geology and Mineral Industries, 800 NE Oregon Street, Portland, OR 97232

JEFFREY A. COE

U.S. Geological Survey, Denver Federal Center, Mail Stop 966, Denver, CO 80225

BAŞAK ŞENER KAYA

Colorado School of Mines, Division of Engineering, Golden, CO 80401

LINA MA

Oregon Department of Geology and Mineral Industries, 800 NE Oregon Street, Portland, OR 97232

Key Terms: ***Multi-Temporal, LiDAR, Landslide, Debris Flow, Accuracy, Oregon, Forested, Differential, Volume, Elevation, Leaf On, Leaf Off, Point Density***

ABSTRACT

We examined elevation changes detected from two successive sets of Light Detection and Ranging (LiDAR) data in the northern Coast Range of Oregon. The first set of LiDAR data was acquired during leaf-on conditions and the second set during leaf-off conditions. We were able to successfully identify and map active landslides using a differential digital elevation model (DEM) created from the two LiDAR data sets, but this required the use of thresholds (0.50 and 0.75 m) to remove noise from the differential elevation data, visual pattern recognition of landslide-induced elevation changes, and supplemental QuickBird satellite imagery. After mapping, we field-verified 88 percent of the landslides that we had mapped with high confidence, but we could not detect active landslides with elevation changes of less than 0.50 m. Volumetric calculations showed that a total of about 18,100 m^3 of material was missing from landslide areas, probably as a result of systematic negative elevation errors in the differential DEM and as a result of removal of material by erosion and transport. We also examined the accuracies of 285 leaf-off LiDAR elevations at four landslide sites using Global Positioning System and total station surveys. A comparison of LiDAR and survey data indicated an overall root mean square error of 0.50 m, a maximum error of 2.21 m, and a systematic error of 0.09 m. LiDAR ground-point densities were lowest in areas with young conifer forests and deciduous vegetation, which resulted in extensive interpolations of elevations in the leaf-on, bare-earth DEM. For optimal use of multi-temporal LiDAR data in forested areas, we recommend that all data sets be flown during leaf-off seasons.

INTRODUCTION

Topographic data from airborne Light Detection and Ranging (LiDAR), also known as Airborne Laser Scanning (Baltsavias, 1999; Wehr and Lohr, 1999) or Airborne Laser Swath Mapping (Harding and Berghoff, 2000; Slatton et al., 2007), have recently become the data of choice for landslide detection and mapping (McKean and Roering, 2004; Schulz, 2004; Glenn et al., 2006; Madin and Burns, 2006; Staley et al., 2006; Ardizzone et al., 2007; McKenna et al., 2008; Scheidl et al., 2008; and Wooten et al., 2008), process studies (Roering et al., 2005; Chen et al., 2006; Corsini et al., 2007; and Dewitte et al., 2008), and hazard assessments and modeling (Baum et al., 2005; Haneberg et al., 2005; and Schulz, 2007). In heavily forested areas, LiDAR data are especially in demand (Haneberg, 2005; Burns, 2007; and Gatziolis and Andersen, 2008) because they can provide unprecedented regional views of the ground surface (Haugerud et al., 2003) that are impossible to obtain from other types of remotely sensed data and that are extremely difficult

to obtain from field surveys. In forested areas, the relative accuracy (i.e., internal consistency between overlapping swaths) of LiDAR data tends to be fairly constant (Gatziolis and Andersen, 2008), although the absolute accuracy of the data is highly variable. This situation is typically not a concern for qualitative landslide inventory mapping applications but can have an adverse impact on landslide process, volumetric, and modeling studies (Haneberg, 2008). These studies often have implications for environmental (e.g., stream sediment and water-supply reservoirs) and landslide hazard problems.

Previous assessments of the absolute accuracies of elevations within single LiDAR data sets in a variety of topographic settings within a range of land covers indicate that root mean square errors (RMSEs) of LiDAR elevations can range from 0.16 to 3.26 m. Adams and Chandler (2002) compared LiDAR data to conventional survey data at the Black Ven landslide on the Dorset coast in the United Kingdom and found that the RMSE of LiDAR elevations was 0.26 m. Bowen and Waltermire (2002) used Global Positioning System (GPS) measurements along the Green River in Utah to document a RMSE of LiDAR elevations of 0.43 m. Hodgson et al. (2003) evaluated LiDAR elevation accuracies for a variety of land covers during leaf-on conditions in North Carolina. Their documented RMSEs were 0.33 m for low grass, 0.37 m for high grass, 1.53 m for scrub/shrubs, 0.45 m for pine tree cover, 1.22 m for deciduous tree cover, and 1.13 m for mixed tree cover. Reutebuch et al. (2003) compared LiDAR data to conventional survey data (collected with a total station) in a conifer forest in western Washington State and found a RMSE of 0.32 m. Their documented mean and maximum (shown in parentheses) differences were 0.16 m (0.61 m) for clear-cuts, 0.18 m (0.41 m) for heavily thinned areas, 0.18 m (0.69 m) for lightly thinned areas, and 0.31 m (1.31 m) for uncut areas. Reusser and Bierman (2007) examined LiDAR data from a bedrock channel of the Susquehanna River in the Appalachian Piedmont and found that raw, unfiltered data provided more accurate elevations than did data that were filtered using Kriging. The RMSEs of unfiltered and filtered data were 1.4 m and 3.26 m, respectively. Haneberg (2008) compared LiDAR-derived 1-m digital elevation model (DEM) elevations to geodetic-level GPS measurements within the City of Seattle, Washington, and found that LiDAR elevation errors had a mean of −0.11 m and a standard deviation (equivalent to RMSE) of 0.75 m.

Multiple airborne LiDAR data sets covering the same geographic area, but from successive time periods (multi-temporal data), have recently become available and are starting to be used for studies of individual landslides (Corsini et al., 2007; Scheidl et al., 2008) and morphometric changes along coastlines (Woolard and Colby, 2002; White and Wang, 2003). The future availability of such data has the potential to provide unprecedented opportunities for studying topographic changes associated with many different types of earth surface processes. However, for regional landslide applications in forested terrain, the potential uses and quality of multi-temporal LiDAR data have not yet been assessed.

In this article, we examined elevation changes detected from two successive sets of LiDAR imagery in a 23-km^2 forested area in the northern Coast Range of Oregon (Figure 1). We evaluated the ability to identify active landslides (landslides that occurred during the time between collections of the two LiDAR data sets) and the vertical accuracy of the elevation changes based on field surveys of recent landslide scars, travel paths, and deposits. One of the two LiDAR data sets was acquired during a leaf-off season and the other during the leaf-on season. Deciduous vegetation in Oregon leafs out during April and loses leaves during November. Therefore, part of our work focused on the impact that leaf-off/leaf-on acquisition times have on the accuracy of detected elevation changes.

BACKGROUND

The study area is located on the eastern flank of the Oregon Coast Range. The area is bisected by Panther Creek, which flows toward the east, between the communities of the City of Carlton and the City of McMinnville, as a tributary to the Willamette River (Figure 1). Therefore, throughout this article we refer to the study area as the Panther Creek study area. The Panther Creek study area consists of the upper portion of the Panther Creek Watershed, which is the extent of the LiDAR data in this region (Figure 1). The smaller drainages (first- and second-order drainages), which generally are tributaries to Panther Creek, Silver Creek, and several other unnamed main drainages, tend to be relatively short, on the order of 300–1,000 m long, and relatively steep, with gradients generally greater than 15°. Elevations in the study area range from 61 m to just over 700 m. The majority of the slopes range from 5° to 45°.

Vegetation in the area primarily consists of a conifer forest, comprised of mainly fir, spruce, cedar, and hemlock trees. In much smaller amounts, and usually occupying low-lying ground adjacent to drainages, deciduous trees, including maple, alders,

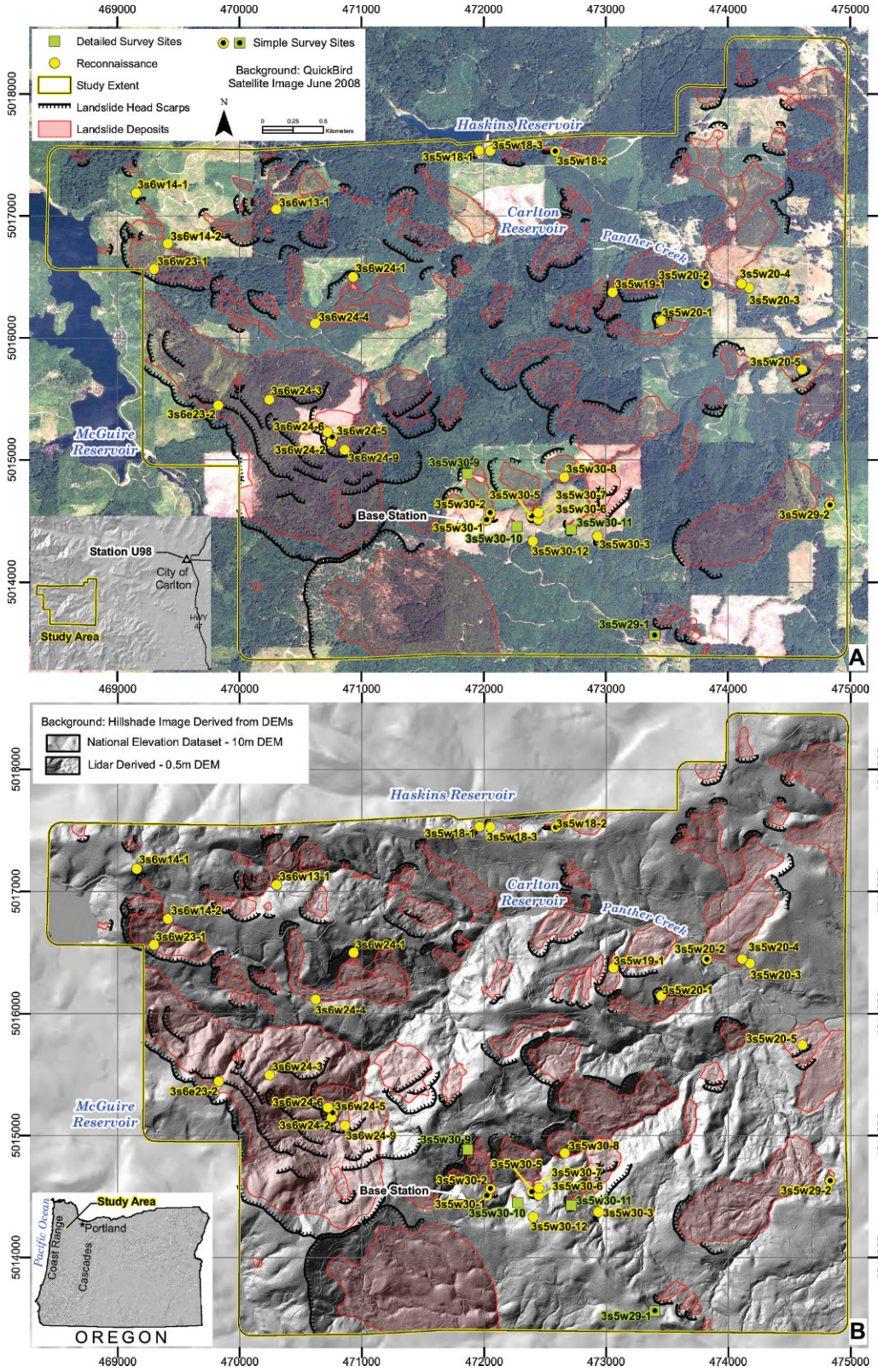

Figure 1. Maps of the Panther Creek study area. Sites visited in September 2008 and historical and prehistoric landslide headscarps and landslide deposits mapped using LiDAR-derived images prior to fieldwork are identified in both (A) and (B). Map A has a QuickBird satellite image base that displays the diversity in land cover (including the range of tree stand ages). Map B has a September 2007 LiDAR-derived hillshade image base that displays drainages, variation in slope gradient, and morphology.

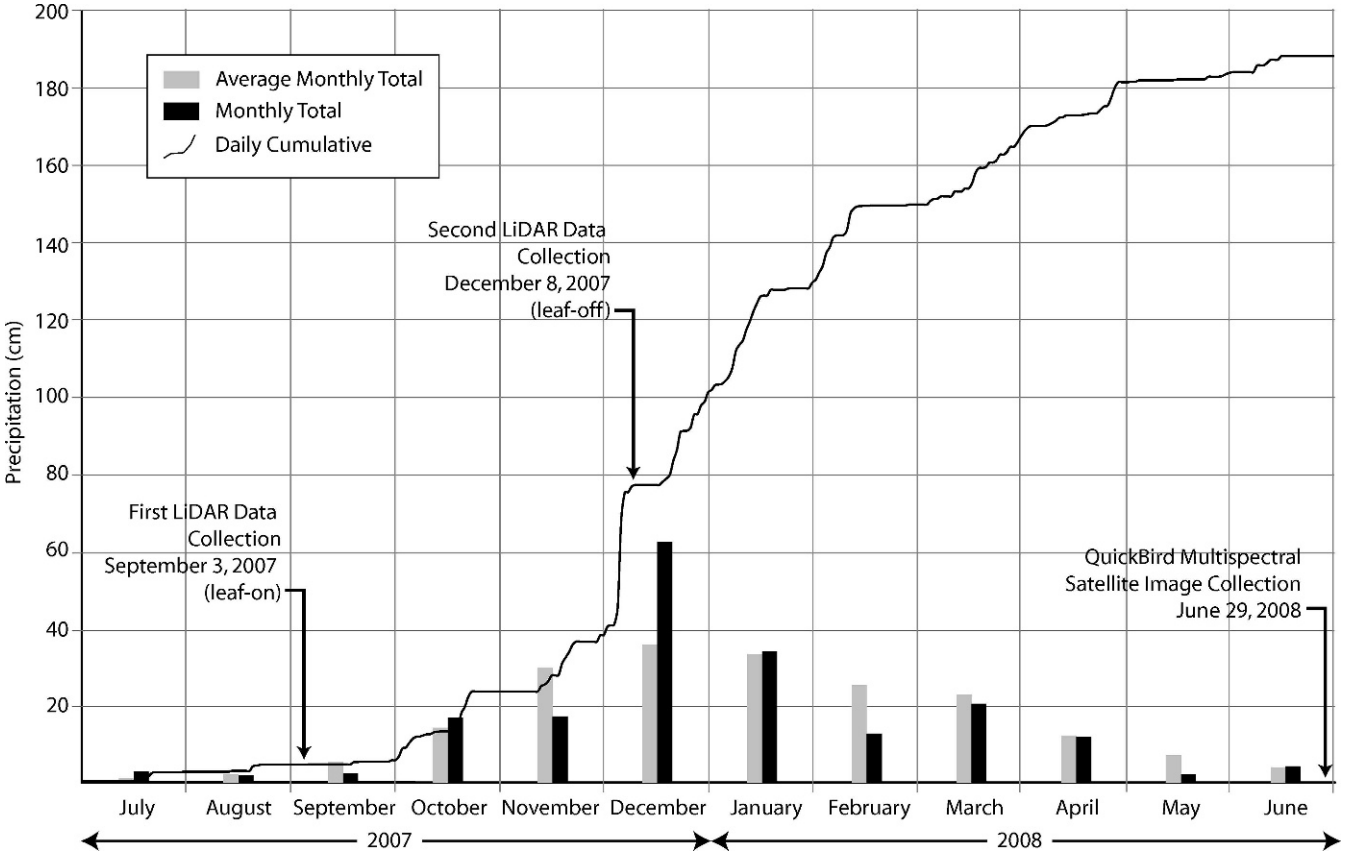

Figure 2. Graph of precipitation with respect to timing of LiDAR data collection between July 2007 and June 2008. The December 8, 2007, LiDAR data were collected right after the large storm of December 2–4, 2007. This storm resulted in more than half (34 cm) of the rainfall total for the month of December 2007 (National Climatic Data Center, 2008).

and cottonwoods, are present. Beneath the canopy and in open areas, giant horsetail, vine maple, salal, devils club, ferns, and Oregon grape are common shrubs (Bureau of Land Management [BLM] and U.S. Forest Service, 1997).

Timber harvesting in the Coast Range is considered some of the most productive in the world, and much of the study area has been harvested multiple times since 1900. Harvesting has resulted in a wide range of tree stand ages throughout the study area (Bureau of Land Management and U.S. Forest Service, 1997) (Figure 1). Based on tree planting data from the BLM, the study area is divided into the following three approximate tree stand age classifications (Bureau of Land Management, 2005):

1. Mature Forest—Generally greater than 20 years old and covering about 70 percent of the study area. Most areas have tree canopy closure and reduced understory vegetation.
2. Young Forest—Generally 5–20 years old and covering roughly 15 percent of the study area. Most areas have dense understory vegetation with poorly developed tree canopy or no canopy.
3. Clear-cut—Generally 0 to 5 years old and covering roughly 15 percent of the study area. These areas have been recently harvested and are often about 0.25 km^2 in size, with recently planted trees or no trees.

Timber management in the study area has resulted in the construction of many actively used roads and old temporary roadbeds. These roads were built by a bulldozer, which drove along a slope and side-casted the excavated material (these roads are often referred to as "cat" roads in the Pacific Northwest). This extensive road network, constructed over the last 100 years, has resulted in numerous slopes that are not engineered and/or engineered cuts and fills with low factors of safety. Many of these older roads were built for temporary access, and, therefore, long-term drainage solutions (e.g., the installation of culverts) were not implemented.

The study area is situated within 80 km of the Pacific Ocean. Climate in the area is strongly influenced by the close proximity to the ocean. Average annual rainfall in the area is about 200 cm (National Climatic Data Center, 2008) (Figure 2).

During storm events, like one that occurred in November 1996, 1-day rainfall totals can be as high as 25 cm within the study area and in the Oregon Coast Range in general (Hofmeister, 2000). During the 3 months between the collection of the two LiDAR data sets (September 3, 2007–December 8, 2007), 72 cm of rainfall was recorded at the dam at Haskins reservoir (Figures 1 and 2). Almost half of the cumulative rainfall (34 cm) in this period occurred during a storm on December 2–4, 2007.

Bedrock underlying the study area is from the middle Eocene Yamhill Formation. The Yamhill Formation is a massive to thin bedded, marine siltstone commonly containing thin tuff and sandstone beds. The surficial portion of the Yamhill Formation tends to be highly weathered and fractured and slakes when exposed to the atmosphere. The Yamhill Formation is intruded with diabase dikes and sills, many of which are exposed at the surface (Wells et al., 1994). On top of weathered bedrock are residual- to colluvial-derived soils that range in thickness from 0 m to ~1 m (Otte et al., 1974). Seven landslides and some isolated Quaternary alluvium (along the lower extent of Panther Creek) were mapped on a 62,500-scale regional geologic map of the area (Wells et al., 1994).

The study area has multiple landowners, including the federal government (BLM), two Oregon cities (McMinnville and Carlton), and private timber companies. Fifty-four percent of the land is private and 46 percent is public. The city lands are all used to collect drinking water that is stored in reservoirs, including the McGuire Reservoir, located along the western edge of the study area; the Haskins Reservoir, located along the northern edge of the area; and the Carlton Reservoir, located in the north-central portion of the area (Figure 1). These reservoirs cover roughly 0.8 percent of the study area.

Multi-Temporal LiDAR Data

The BLM contracted Watershed Sciences, Inc., to collect airborne LiDAR data of the study area on September 3, 2007 (leaf-on), and again on December 8, 2007 (leaf-off). Both data sets were collected using identical acquisition and processing methods. A Leica ALS50 Phase II laser was used to acquire ≥105,000 laser pulses per second (i.e., 105-kHz pulse rate) with a scan swath of 28° in a downward direction below the aircraft (i.e., a swing of 14° normal to the flight direction about a vertically downward-oriented axis). These instrument settings yielded an emitted laser pulse density of ≥8 points per square meter. The aircraft position was measured twice per second (2 Hz) by an onboard differential GPS unit. Aircraft attitude was measured 200 times per second (200 Hz) as pitch, roll, and yaw (heading) from an onboard inertial measurement unit (Watershed Sciences, 2008).

A GPS-based ground survey consisting of hundreds (524) of real-time kinematic (RTK) points was conducted at the same time as the airborne LiDAR data collection. The LiDAR data points were processed and tested for accuracy against the RTK survey points. LiDAR points above the ground surface were identified and removed using automated and manual methods to create a data set containing ground points. Automated identification and removal of points above the ground was done using TerraScan software (Soininen, 2004). Manual identification and removal of points above the ground followed the automated method and consisted of visual inspection and editing, particularly in areas where the TerraScan automated methodology was known to be deficient (e.g., cliffs, incised stream banks, dense vegetation; also see McKenna et al., 2008). For the leaf-on and leaf-off data sets, the average pulse density was 9.25 points/m^2 and 9.15 points/m^2, respectively. The average density of ground-classified points was 0.52 points/m^2 and 0.84 points/m^2 for leaf-on and leaf-off data sets, respectively. First-return (above-ground) points, sometimes called highest-hit points, and the ground-classified points were used to create separate triangulated irregular networks (TINs) that were converted into 0.5-m pixel (grid) DEMs (a first-return DEM and a bare-earth DEM) (Watershed Sciences, 2008).

The horizontal datum and coordinate system for all LiDAR data were the North American Datum of 1983 (NAD83) and the Universal Transverse Mercator (UTM), zone 10, coordinate system (meters), respectively. Elevations were provided as mean sea level elevations (meters) in the North American Vertical Datum of 1988 (NAVD88) and utilized the GEOID03 model from the National Geodetic Survey (Watershed Sciences, 2008).

The reported vertical, absolute RMSE (deviation between elevations of the RTK survey points and LiDAR points) of both LiDAR data sets used in this study was 0.02 m (Watershed Sciences, 2008). Watershed Sciences states that this accuracy should be considered only for areas comprising permanent flat hard surfaces and no vegetation (e.g., open paved roads). The part of the study area with these surface characteristics is very small (roughly 1 percent).

METHODS

We evaluated the suitability of the two successive sets of LiDAR data for identifying active landslides and the vertical accuracy of detected elevation

changes based on a comparison to field surveys at active landslides. Active landslides are defined in this article as those that experienced movement between September 2007 and December 2007. In order to evaluate the LiDAR data, three primary tasks were performed: 1) Geographic Information System (GIS) mapping, 2) ground-based site reconnaissance visits (28 sites) and/or simple site surveys (eight sites), and 3) ground-based detailed GPS and total station surveys (four sites). GIS-based mapping consisted of three parts: 1a) mapping predominately inactive (historical and pre-historic landslides), 1b) mapping probable active landslides, and 1c) calculation of spatial attributes for verified active landslides.

To evaluate and compare elevations between the two sets of LiDAR data, as well as the elevations between LiDAR and survey data, we calculated elevation difference values at individual cell or profile point locations and then aggregated these values by computing RMSEs, systematic errors, and maximum difference values for the differential LiDAR data set, individual profiles, or each individual landslide site that was surveyed with the total station. RMSEs were calculated using the frequently used (Slama et al., 1980), common equation for RMSE:

$$RMSE = \sqrt{\frac{\sum_{i=1}^{n} (Xa_i - Xb_i)^2}{n}},$$

where Xa and Xb are elevations from data sets a (e.g., December 2007 LiDAR) and b (e.g., September 2007 LiDAR) and n is the total number of elevations in each data set.

Systematic errors are commonly defined as errors or biases in measurements that occur in a definite pattern (Slama et al., 1980). We define systematic error (SE) as the average of elevation differences in two data sets and calculate SE using the following equation:

$$SE = \frac{\sum_{i=1}^{n} (Xa_i - Xb_i)}{n}.$$

Even though the terms RMSE and SE indicate that we are evaluating errors, in this article, as in many previous studies mentioned in the Introduction, we use RMSE and SE to evaluate elevation differences between data sets where neither data set represents an exact (true) value. Therefore, for some readers, it may be helpful to think of our RMSE and SE as a standard deviation of elevation differences, and mean bias of elevation differences, respectively.

GIS-Based Mapping

We initially mapped landslide deposits and scarps (head and lateral) using the September 2007 LiDAR data (Figure 1). This mapping was done in a GIS using shaded relief maps (hillshades), a slope map, a topographic contour map, ground-surface profiles, and a June 2008 QuickBird satellite image with a 2.5-m cell size. (QuickBird and ArcMap are registered trademarks of DigitalGlobe, Inc., and ESRI, Inc., respectively. Any use of trade, product, or firm names is for descriptive purposes only and does not imply endorsement by the U.S. Government.) Utilization of complementary data sets has been previously shown to be reliable for accurately mapping landslides from LiDAR data (Schulz, 2004; Burns, 2007; and McKenna et al., 2008). Because landslides in the study area are of various sizes, mapping was done at several different scales, including the following scales: 1:24,000, 1:10,000, and 1:4,000. The protocol developed by Burns and Madin (2009) was followed to map these landforms. Nearly all (greater than 98 percent) of the landslides mapped using this method were found to be inactive.

To test the suitability for locating active landslides using the multi-temporal LiDAR data, a computer-based assessment was carried out. The first LiDAR data set (September 2007, leaf-on) was subtracted from the second set (December 2007, leaf-off) to create an elevation-difference data set. In this data set, negative values represented decreases in elevation and positive values represented increases in elevation from September to December. The results shown on this map are referred to as differential data throughout the article. To calculate statistics on this differential DEM, we used only non-water areas which included inactive landslides (i.e., we removed all area encompassed by the three drinking water reservoirs area and active landslide areas). This 0.5-m resolution differential DEM contained 98,325,141 cells and had overall RMSE, SE, and maximum negative and positive values of 0.28 m, −0.11 m, −8.31 m, and 12.68 m, respectively. The differential data set has values of elevation change throughout 98 percent of the study area. Seventy-two percent of the area had negative elevation changes and 26 percent had positive changes. From field observations, we knew that the large percentage of apparent elevation changes was a gross overestimate of actual elevation changes within the area. So we tested multiple cutoff (threshold) values for removing noise within the differential data set to increase our ability to locate probable landslides. Threshold values close to zero (starting with ±0.02 m, the RMSE value reported by Watershed Sciences [2008]) were used to sequentially

remove data from the differential data set. These threshold values included the following: ±0.02 m, ±0.15 m, ±0.28 m, ±0.50 m, and ±0.75 m (Figure 3). The percentages of the study area that showed changes in elevation for each of these threshold values were 95 percent, 53 percent, 19 percent, 10 percent, and 4 percent, respectively. The five data sets (±0.02 m, ±0.15 m, ±0.28 m, ±0.50 m, and ±0.75 m) were visually examined, and two differential data sets were selected (those with thresholds of ±0.50 m and ±0.75 m) and used to map probable active landslide areas to be checked in the field (Figure 3). The differential data sets that used the ±0.50-m and ±0.75-m threshold values were selected because these threshold values eliminated obvious areas of differential noise, that is, areas with widespread contiguous negative or positive changes or visually speckled patterns caused by both positive and negative elevation changes. The ±0.75-m threshold value eliminated more noise than the ±0.50-m value, but we used both thresholds for mapping to be sure that we did not remove any probable landslide areas through the exclusive use of the ±0.75-m value.

The selection of these threshold values is further supported by landslide depth data from a database of 9,582 landslides in Oregon that occurred during the period from 1996 to 1997 (Hofmeister, 2000). Out of the 9,582 landslides, 1,487 included recorded depths. Eighty-eight percent of these depths were greater than 0.50 m. The threshold value of 0.50 m also helped us to distinguish active landslides from rills and gulleys caused by erosion from surface water runoff (generally less than 3 dm in depth).

Mapping from these two data sets consisted of outlining probable active landslide areas (Figure 3) and giving each area a high or low confidence value. The confidence level was based primarily on the presence or absence of the following parameters:

1. Contiguous positive or negative data in a downslope direction.
2. Presence of negative elevation change in an upslope area with a positive change immediately downslope.
3. Identification of a probable active landslide on the June 2008 QuickBird image.

High confidence was applied if one or more of these three parameters were present. If none of these parameters were present then a low confidence level was assigned.

This mapping identified relatively large (generally >10,000 m^2), deep-seated landslides and channelized debris flows, including scars (initiation sites), travel paths, and deposits. These probable active landslides were then checked in the field using one of three methods: reconnaissance, simple surveys, and/or detailed surveys.

Once the active landslides were located and polygons were created in a GIS, we calculated spatial attributes of each polygon, including 1) area; 2) raw and corrected negative, positive, and net volumes; 3) average pre-failure slope angle; 4) depth to failure surface; and 5) maximum negative elevation change. All of these calculations were done in ArcMap GIS, version 9.3. Corrected volumes were calculated using a differential DEM shifted upward in elevation by 0.11 m to account for the SE of −0.11 m. The average pre-failure slope angle and the depth to the failure surface were estimated using procedures outlined by Burns and Madin (2009). The slope angle was estimated through measurement of the slope directly adjacent to the landslide. The depth to the failure surface was estimated by multiplying the vertical height of the scarp (the average difference in elevation between the bottom and top of the headscarp measured on the December 2007 LiDAR DEM) by the cosine of the slope angle to yield the depth perpendicular to the slope. A secondary estimate to the depth of failure surface was calculated by multiplying the maximum negative elevation change (between the September 2007 and December 2007 bare-earth LiDAR DEMs) within the boundaries of each landslide by the cosine of the slope angle. This secondary estimate was especially useful for shallow landslides where most of the material was evacuated from the scar area.

Ground-Based Site Reconnaissance Visits and Simple Site Surveys

In order to assess whether the GIS-based mapping succeeded in identifying active landslides, we conducted field-based reconnaissance at 33 sites in September 2008. Simple site surveys were conducted at eight of the 33 sites.

Field-based reconnaissance consisted of verifying the presence or absence of an active landslide by looking for the presence or absence of fresh landslide characteristics or morphologies. Documentation at each site consisted of recording basic landslide data, including dimensions, type of material, type of movement, surrounding vegetation, and possible causes. If a landslide was not present, documentation of possible reason(s) for misidentification were recorded, including type and height of vegetation, presence and characteristics of erosion, and human-related activities.

Simple site surveys consisted of measuring downslope profiles (Hall et al., 1994) using a tape measure and clinometer at ground reconnaissance sites where

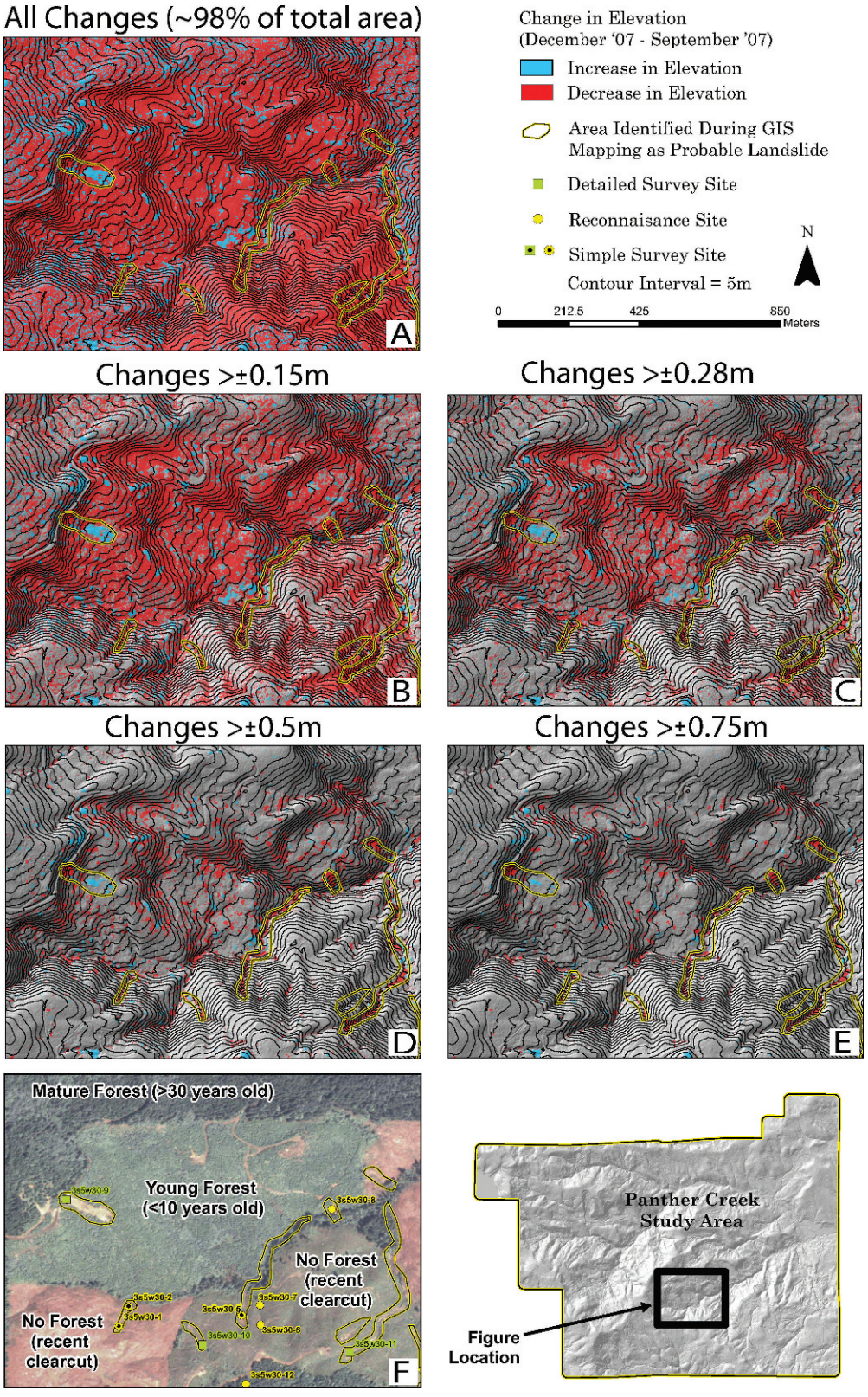

Figure 3. Maps showing the reduction in spatial extent of elevation changes in the differential data set as a function of threshold values. (A) Raw differential data set with no threshold value. (B–E) Maps showing elevation changes greater than ±0.15 m, ±0.28 m, ±0.50 m, and ±0.75 m, respectively. (F) Quickbird image showing variation in tree stand age for the area. Differential data sets with threshold values of ±0.50 m and ±0.75 m were used to located probable landslide areas.

active landslides were identified. Elevations of pre-failure landslide surfaces were estimated in the field. The method resulted in a profile and plan-view map at each site.

The profile data from simple site surveys were compared to profiles generated using the two LiDAR data sets. The simple site survey data have a much lower spatial resolution (generally about 1 point per 10 m horizontal) than the LiDAR-derived DEM (0.5-m horizontal grid spacing); thus, only two key parameters were examined: horizontal extent of primary elevation change areas (e.g., landslide scar areas with a decrease in elevation and toe areas with an increase in elevation) and the average elevation change within each of these areas (Figure 4). This comparison was performed at all eight simple site survey locations.

Detailed Surveys Using a GPS and Total Station

In September 2008, detailed surveys of elevations at four landslide sites (Figure 1, sites 3s5w29-1, 3s5w30-10, 3s5w30-11, and 3s5w30-9) were done using Ashtech dual-frequency GPS receivers and a Topcon total station surveying unit. At each site, two control points were installed and surveyed with the GPS equipment using static surveying techniques with differential positioning. We used two receivers for the GPS survey, one receiver positioned at a base station within the study area (point "Base Station," Figure 1) and one receiver moving to control points at the four individual landslide sites. The position of the base station was determined by a static GPS survey using a benchmark (Station Designation U98) located in the town of Carlton, which is located about 14 km northeast of the landslide sites, as a base station (point U98, inset map of Figure 1). The position of station U98 was determined by a GPS survey performed by Washington County, Oregon, personnel in 2000. The coordinates that we used for U98 were from the National Geodetic Survey's datasheet webpage (http://www.ngs.noaa.gov/cgi-bin/datasheet.prl).

All GPS data were post-processed using Ashtech Solutions software, version 2.70. Baselines and point positions were calculated from the base station (point Base Station, Figure 1) for each of the eight control points. All baselines were less than 2 km in length. Standard errors of computed point positions were derived using Ashtech Solutions and were less than 1 cm in horizontal and 1.5 cm in vertical (elevation). In order to directly compare our detailed survey data to the LiDAR data, horizontal coordinate positions for all control points were transformed into the NAD83 datum and then projected into the UTM, zone 10 coordinate system. GPS ellipsoid heights (i.e., elevations) of control points were transformed into mean sea level elevations in the NAVD88 datum using the GEOID03 model by the National Geodetic Survey.

After the eight control points were surveyed using GPS, we used the UTM coordinates and mean sea level elevations to orient the Topcon total station at each site. At each site, the instrument was set up over one of the control points, and the other control point was used as a backsight point. Once the total station was set up and oriented, we surveyed four or five topographic profiles at each site using a fixed-height prism pole. One profile was done along the maximum length of each landslide (i.e., a longitudinal profile), and another three or four profiles were done across the width of each landslide (i.e., cross sections).

Based on previous experience with this type of total station survey using a prism pole in open areas (i.e., clear-cuts), the relatively short shot lengths between the total station and the profile points (always less than 300 m) and the precision specifications stated by Topcon for the total station instrument (± 1 second for horizontal and vertical angles, $\pm$[2 mm + 2ppm $\times$ shot distance] for distance measurements), we estimate that elevation error of individual surveyed profile points at 0.03 m.

Once surveyed, profile data were imported into ArcMap GIS and overlain directly on the LiDAR data. At each profile point, elevations at the underlying 0.5-m LiDAR cells were extracted from ArcMap. Elevations were extracted from the bare-earth and first-return DEM data from the September 2007 and December 2007 LiDAR flights.

RESULTS

GIS-Based Mapping

Our map of historical and prehistoric landslides from the September 2007 LiDAR data includes 93 landslide deposits, which cover about 28 percent of the Panther Creek study area (Figure 1). The largest mapped deposit covers an area of 2,052,830 m^2, and the smallest covers an area of 384 m^2. These landslides were classified as earth/debris slides (12 percent), earth flows (68 percent), debris flows (12 percent), or complex slope movements (8 percent) (see Varnes [1978] for a further description of these landslide types). Fifty-three of the landslides were classified as historical and 36 as prehistoric. Only two of these 93 landslide deposits were found to have been active between the collection of the two LiDAR data sets. Both of these landslides represented reactivations of older landslides. The average estimated pre-failure

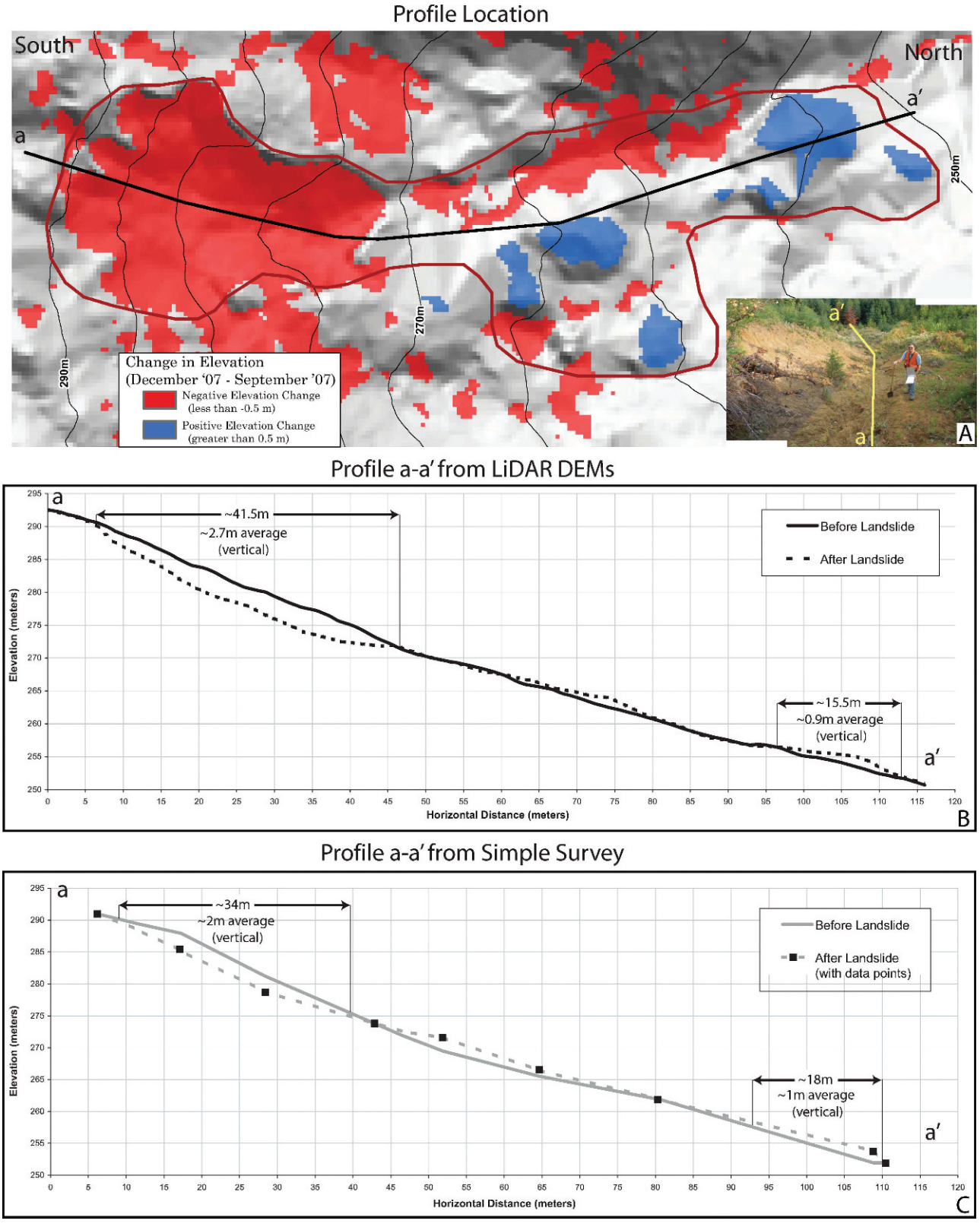

Figure 4. Comparison between LiDAR data and simple survey data at site 3s5w29-2. (A) Map showing areas of negative elevation changes (red colors, landslide depletion areas) and positive elevation changes (blue colors, landslide deposition areas) derived from differential LiDAR data. Inset shows photo taken looking downslope along profile a-a′. Landslide deposit is located in the upper center of the photo (near the dead Douglas fir trees with brown needles). (B) Profile data from the leaf-on and leaf-off LiDAR data sets. (C) Profile data from simple survey. "After landslide" surface was collected by simple survey, and "before landslide" surface was estimated during the simple survey.

slope angle in landslide source areas was 22°. The maximum slope angle in source areas was 45°. Ninety-eight percent of estimated depths to failure surfaces ranged from roughly 4 m to 50 m, with an average of 15 m. There were two landslides with estimated depths between roughly 80 m and 100 m. Debris-flow fans were found on slopes ranging from 5° to 12° and had estimated depths ranging from 5 m to 15 m.

Based on our mapping from the differential LiDAR data sets and QuickBird imagery, we identified 40 probable active landslides in the study area. We visited 28 of the 40 sites in the field, as well as five additional sites that were identified from fieldwork alone (Table 1). Prior to fieldwork, we ranked the presence of landslides at 16 of the 28 sites with high confidence and at 12 of the sites with low confidence (Table 1). We verified active landslides at 15 (54 percent) of the total 28 sites. However, 14 (88 percent) of the high-confidence sites and one (8 percent) of the low-confidence sites were verified as active landslides in the field (Table 1).

At two-thirds of the verified sites, the relative forest age was either mature or clear-cut. The other one-third of sites were covered by young forest. Additionally, seven of the 13 (54 percent) misidentified landslide sites were in young forest areas, and six (46 percent) were in mature forests. None were in clear-cuts. Therefore, we suspect that the presence, age, and type of vegetation at each site, or the change in this vegetation from leaf-on to leaf-off, affected our ability to correctly identify active landslides from the differential LiDAR data set.

We investigated the possible reasons the two sites with high confidence were falsely identified as landslides. At one of these two sites (3s5w19-1), elevation differences were found to result from roughly 1.5 m of erosion around a 30-cm culvert outlet, which could not have been distinguished from a landslide without field verification. At the other falsely identified site (3s6w13-1) we found a combination of young forest and deciduous vegetation (alder and devils club).

Additionally, we investigated the possible reasons for the false identification of landslides at the sites with low confidence by collecting vegetation data at both the verified and falsely identified sites (Table 1). At 11 of the 12 (92 percent) low-confidence sites, we found relatively short (<5-m), deciduous vegetation, including vine maple, devils club, and young alder trees. These types of vegetation are dense and likely cause a large reduction in LiDAR ground-point densities during leaf-on season and a subsequent increase in ground-point densities during leaf-off season. This situation resulted in elevation changes in the bare-earth differential LiDAR data set that were not due to actual changes in the ground surface.

Five active landslides had not been identified during the GIS mapping prior to fieldwork yet were found in the field (Table 1; GIS mapping confidence = NA). Two of these five sites (3s5w30-7 and 3s5w30-6) were found to lack all three factors (contiguous data, presence of adjacent negative and positive elevation change, and identification on the QuickBird imagery) used to identify them as probable landslides with high confidence. A third site (3s6w24-6) had roughly 15 cm of vertical displacement and therefore was below the ±0.50-m and ±0.75-m threshold values. The other two sites (3s6w24-2 and 3s6w24-5) were in a clear-cut but were simply not visible in the LiDAR or QuickBird imagery.

Ground-Based Surveys

Results from the simple site surveys are given in Table 2, and an example of a comparison of these results to the two LiDAR data sets is given in Figure 4. The average elevation difference in zones of depletion and accumulation between the LiDAR DEMs and the simple site surveys was 0.5 m. The average difference in horizontal distance between the zone of depletion and accumulation was 3.7 m.

One of the sites (3s5w29-1) was surveyed by both simple survey and detailed total station survey methods. In the source area of this landslide, the maximum elevation change in the differential LiDAR was −3.54 m. In the simple survey, we found roughly −2 m of maximum elevation change. In the detailed GPS and total station survey, we found a maximum of about −2.5 m of elevation change.

Statistics for active landslides that were verified in the field are given in Table 3. The total area of active landslides was about 59,000 m^2. Two rotational landslides had volume increases (3s5w24-5 and 3s5w20-1), but all other landslides had volume decreases. The total corrected net volume change for all polygons was about −11,700 m^3 (Table 3). About 80 percent of this missing material was from debris-flow and earth-flow sites. One probable cause of missing material, especially from flows in or near drainages, was removal by erosion either during or after the failure. During our fieldwork, we noted that material in many debris-flow sites had traveled into the stream system and out of the local polygon areas (e.g., see Figures 5–8). Also, some landslide areas had signs of significant post-deposition erosion or a complete lack of a discrete deposition area. All of these situations would result in negative net volumes in Table 3. However, some landslides did not occur in or near drainages and may have some volume loss related to contraction or compaction of material, especially in the cases where the majority of the

Table 1. *Reconnaissance and simple survey results from 33 field sites.*

Site ID No.	GIS Mapping Confidence (High or Low)	Type of Fieldwork	Landslide Verified in Field (Yes or No)	Relative Forest Age	Comment(s)
3s5w19-1	High	Reconnaissance	No	Mature	Douglas fir; 1.5-m–deep erosion from culvert outfall
3s6w13-1	High	Reconnaissance	No	Young	Alder and devils club
3s5w18-1	High	Reconnaissance	Yes	Young	Douglas fir, alder
3s5w18-2	High	Reconnaissance, simple survey	Yes	Young	Douglas fir, vine maple, alder, ferns
3s5w20-1	High	Reconnaissance	Yes	Young	Douglas fir
3s5w20-2	High	Reconnaissance, simple survey	Yes	Mature	Mixed maple and Douglas fir
3s5w29-1	High	Reconnaissance, simple survey, detailed survey	Yes	Mature	Recently thinned but mature Douglas fir
3s5w29-2	High	Reconnaissance, simple survey	Yes	Young	Douglas fir
3s5w30-1	High	Reconnaissance, simple survey	Yes	Clear-cut	—
3s5w30-10	High	Reconnaissance, detailed survey	Yes	Clear-cut	—
3s5w30-5	High	Reconnaissance, simple survey	Yes	Clear-cut	—
3s5w30-11	High	Reconnaissance, detailed survey	Yes	Clear-cut	—
3s5w30-2	High	Reconnaissance, simple survey	Yes	Clear-cut	—
3s5w30-8	High	Reconnaissance	Yes	Young	Douglas fir
3s5w30-9	High	Reconnaissance, detailed survey	Yes	Young	Douglas fir
3s6w24-1	High	Reconnaissance	Yes	Mature	Douglas fir
3s5w18-3	Low	Reconnaissance	No	Mature	Very little vegetation (ferns), near-vertical rock cliff
3s5w20-3	Low	Reconnaissance	No	Young	1.5- to 3-m–tall vine maple
3s5w20-5	Low	Reconnaissance	No	Young	Alder, maple, isolated Douglas fir
3s6e23-2	Low	Reconnaissance	No	Young	Alder, devils club
3s6w13-2	Low	Reconnaissance	No	Mature	Alder, devils club
3s6w14-1	Low	Reconnaissance	No	Young	3-m–tall vine maple
3s6w14-2	Low	Reconnaissance	No	Young	3-m–tall vine maple, 10-m–tall alder
3s6w23-1	Low	Reconnaissance	No	Young	Alder, devils club
3s6w24-3	Low	Reconnaissance	No	Mature	Vine maple, devils club
3s6w24-4	Low	Reconnaissance	No	Mature	1.5- to 3-m–tall vine maple and alders
3s6w24-9	Low	Reconnaissance	No	Mature	Alder, devils club
3s5w30-3	Low	Reconnaissance	Yes	Clear-cut	—
3s5w30-7*	NA	Reconnaissance	Yes	Clear-cut	Area lacked three confidence parameters on differential data set
3s5w30-6*	NA	Reconnaissance	Yes	Clear-cut	Area lacked three confidence parameters on differential data set
3s6w24-5*	NA	Reconnaissance	Yes	Clear-cut	Recent clear-cut (sometime after 2004)
3s6w24-2*	NA	Reconnaissance, simple survey	Yes	Clear-cut	Recent clear-cut (sometime after 2004)
3s6w24-6*	NA	Reconnaissance	Yes	Clear-cut	15-cm drop in road fill embankment; Not detected in 0.5-m or 0.75-m differential

GIS = Geographic Information System; NA = not applicable.
*These five landslides were located in the field randomly. None of these areas was identified as a probable landslide during GIS work.

material initiated from loose, road-fill embankments. In other cases, the apparent missing material was probably caused by local large negative systematic elevation errors in the differential DEM due to local vegetation types. For example, the area with young forest around site 3s5w30-9 had a local SE of −0.30 m. The net volume change for this site was −2,730 m^3 using the raw DEM, about −2,069 m^3 using the corrected DEM, and about −920 m^3 using a differential DEM corrected using the local SE of −0.30 m. Thus, we estimate that some of the net volumes for individual sites (both raw and corrected) probably have volumetric errors much larger than those shown in Table 3. More fieldwork at individual landslide sites would be needed before the volumes shown in Table 3 could be used in landslide process or hazards studies.

The average estimated pre-failure slope angle for all active landslides was 35°, and the calculated average pre-failure slope angle from the September (leaf-on) LiDAR data set was 29° (Table 3). The average estimated depth to the failure surface was 2.9 m, and the average of secondary estimates of depth to failure was 3.0 m (Table 3).

A large difference tends to exist between pre-failure slope angles and LiDAR slope angles shown in

Table 2. *Summary of differences between December 2007 LiDAR DEM and simple surveys.*

Site ID No.	Data Collection Method	Total Horizontal Distance (m)	Primary Zone of Depletion		Primary Zone of Accumulation	
			Horizontal Distance (m)	Average Vertical Change (m)	Horizontal Distance (m)	Average Vertical Change (m)
3s5w29-2*	LiDAR DEM	109.0	41.5	−2.7	15.5	0.9
	Simple survey	102	34	−2	18	1
3s6w24-2	LiDAR DEM	29.9	12.5	−2.6	11.3	1.0
	Simple survey	27	11	−1.5	8	1
3s5w29-1†	LiDAR DEM	45.1	16.2	−2.2	16.5	0.6
	Simple survey	35	13	−1.5	10	0.5
3s5w30-5‡	LiDAR DEM	127.6	22.2	−2.7	ND	ND
	Simple survey	102	22	−1	ND	ND
3s5w20-2	LiDAR DEM	42	27	−1.6	15	0.8
	Simple survey	46	29	−1	17	0.76
3s5w30-1§	LiDAR DEM	39	17	−1.7	ND	ND
	Simple survey	43	16	−1.5	ND	ND
3s5w18-2§	LiDAR DEM	15.5	10.7	−1.2	ND	ND
	Simple survey	6.5	6.5	−0.6	ND	ND
3s5w30-2	LiDAR DEM	24.6	19	−1.5	2.3	0.3
	Simple survey	28	10	−0.9	7	0.6

LiDAR = Light Detection and Ranging; DEM = digital elevation model; ND = no data.
*Site included in Figure 4.
†Site surveyed by simple and detailed methods.
‡ND; Site 3s5w30-5 deposit was likely removed by stream erosion prior to LiDAR or simple surveys.
§ND; Sites 3s5w30-1 and 3s5w18-2 landslide deposits were removed from roadways prior to LiDAR or simple surveys.

Table 3. But most of the landslides with the largest differences are debris flows, which tend to have long travel paths and deposit areas. Thus, the large differences in slope angles were caused by the inherent difference in measurement methods. That is, pre-failure slope angles were measured only in the scar area, and the average slope from the LiDAR was calculated over the entire length of the landslide, including scar, travel path, and deposit.

Detailed GPS and Total Station Surveys

Results from our detailed surveys at the four landslide sites are given in Figures 5 through 8 and Table 4. Overall, we surveyed 285 points along 18 profiles at the four sites. A comparison of elevations from the total station measurements with those from the December 2007 bare-earth DEM indicate an overall RMSE of 0.50 m (for the 285 points), a maximum error of 2.21 m, and an SE of 0.09 m (Table 4, last row). Results from our analysis at each site are given below.

At site 3s5w30-9 (Figure 5), a large landslide occurred between September 2007 and December 2007 (Figure 9). The landslide resulted from a failure of fill material underlying an active logging road through a forested area. A drainage culvert was present at the site and was visible in the landslide deposit when we visited in September 2008. Elevation changes caused by this landslide are visible when comparing profiles derived from bare-earth LiDAR data from September 2007 and December 2007 (Figure 5). Maximum elevation changes were about 6 m in the landslide source area (Figure 5, profiles A-A′ and B-B′) and about 1 m in the relatively flat deposition area (Figure 5, profiles C-C′ and D-D′). The maximum elevation changes in the source area at this landslide represented some of the largest changes within the differential LiDAR data in the entire Panther Creek study area. The September 2007 bare-earth LiDAR-derived DEM was subtracted from the September 2007 first-return DEM in order to evaluate vegetation cover. The differential DEM indicates that tree cover in the area prior to the landslide ranged from 4 to 8 m in height (Figure 5), which is in agreement with field observations of tree heights surrounding the landslide in September 2008 (Figure 9). These tree heights are consistent with a young forest (e.g., Figure 3F). A comparison of post-landslide, bare-earth LiDAR data from December 2007 and total station survey data from September 2008 indicate that the overall RMSE of bare-earth LiDAR data at the site is 0.27 m (site 3s5w30-9, All profiles; Table 4). RMSEs of individual profiles at the site range from 0.17 to 0.33 m. The maximum error (1.30 m) is along profile A-A′ and is at the lip of the retrogressing headscarp, but it is in the opposite direction of what would be expected if the error was caused by real elevation changes due to retrogression. That is, the error is positive, indicating that the

Table 3. *Summary of data for active landslides. Two standard deviation (SD) volumetric errors (0.56 m) were estimated using 2 times the 0.28-m root mean square error (RMSE; equivalent to 1 SD) of our differential Light Detection and Ranging (LiDAR) digital elevation model (DEM), and the areal extent of individual landslide sites, in eq. 5 of Coe et al. (1997). This error calculation assumes a negligible systematic error (SE) within the differential DEM.*

Site ID No.	Movement Classification	Total Area (m^2)	Average Estimated Pre-Failure Slope Angle (°)	Average Slope from LiDAR (°)	Estimated Depth to Failure Surface from Headscarp (slope normal) (m)	Estimated Depth to Failure Surface from Maximum Elevation Change (slope normal) (m)	Positive		Negative		Change	
							Raw Volume (m^3) ± 2SD	Corrected Volume (m^3) ± 2SD	Raw Volume (m^3) ± 2SD	Corrected Volume (m^3) ± 2SD	Raw Net Volume (m^3) ± 2SD	Corrected Net Volume (m^3) ± 2SD
3s5w18-1	Earth translational slide	1,261	30	37	−2.6	−1.9	102 ± 4	132 ± 5	−388 ± 9	−279 ± 9	−286 ± 10	−147 ± 10
3s5w18-2	Earth flow	809	45	47	−3.5	−1.4	41 ± 4	132 ± 4	−295 ± 7	−228 ± 7	−254 ± 8	−96 ± 8
3s5w20-1	Earth rotational slide + earth flow	28,942	15	16	−6.9	−4.0	3,907 ± 31	5,551 ± 38	−5,479 ± 37	−3,940 ± 31	−1,573 ± 49	1,611 ± 49
3s5w20-2	Earth flow	756	20	22	−2.6	−3.3	156 ± 5	185 ± 5	−533 ± 7	−478 ± 6	−377 ± 8	−294 ± 8
3s5w29-1	Earth flow	564	40	28	−2.6	−3.2	98 ± 4	124 ± 5	−310 ± 5	−274 ± 5	−212 ± 7	−149 ± 7
3s5w29-2	Earth flow	3,081	28	23	−3.5	−3.6	264 ± 7	347 ± 9	−2,194 ± 14	−1,938 ± 7	−1,930 ± 16	−1,591 ± 16
3s5w30-1	Debris flow	199	50	39	−1.7	−2.9	0 ± 0	0 ± 0	−246 ± 4	−224 ± 4	−246 ± 4	−224 ± 4
3s5w30-10	Debris flow	526	35	26	−4.3	−3.0	70 ± 3	82 ± 3	−492 ± 6	−446 ± 6	−422 ± 7	−364 ± 7
3s5w30-5	Debris flow	1,073	42	40	−4.3	−3.0	0 ± 0	0 ± 1	−1,694 ± 9	−1,576 ± 9	−1,694 ± 9	−1,576 ± 9
3s5w30-11	Debris flow	3,220	45	30	−2.6	−4.5	305 ± 6	349 ± 6	−4,445 ± 15	−4,134 ± 15	−4,139 ± 16	−3,785 ± 16
3s5w30-2	Debris flow	218	30	21	−1.7	−2.1	19 ± 3	28 ± 3	−118 ± 3	−104 ± 3	−100 ± 4	−76 ± 4
3s5w30-8	Earth flow	2,075	35	32	−2.6	−2.6	114 ± 6	170 ± 7	−1,152 ± 12	−980 ± 11	−1,038 ± 13	−810 ± 13
3s5w30-9	Earth flow	6,012	40	15	−5.2	−7.0	1,289 ± 15	1,632 ± 17	−4,019 ± 16	−3,701 ± 15	−2,731 ± 22	−2,069 ± 22
3s5w24-1	Earth rotational slide + earth flow	7,386	25	26	−5.2	−5.4	1,544 ± 15	1,908 ± 18	−4,013 ± 19	−3,564 ± 17	−2,469 ± 25	−1,656 ± 25
3s5w30-3	Earth flow	182	30	34	−2.6	−1.7	1 ± 0	1 ± 1	−151 ± 4	−131 ± 4	−150 ± 4	−130 ± 4
3s5w30-7	Earth flow	279	35	29	−1.7	−1.7	11 ± 3	22 ± 3	−92 ± 4	−72 ± 3	−81 ± 5	−50 ± 5
3s5w30-6	Earth flow	398	35	34	−1.7	−2.2	18 ± 3	28 ± 3	−250 ± 5	−217 ± 5	−232 ± 6	−189 ± 6
3s5w24-5	Earth rotational slide	930	35	33	−0.9	−1.5	205 ± 6	248 ± 6	−257 ± 7	−198 ± 7	−52 ± 9	51 ± 9
3s5w24-2	Earth rotational slide	348	40	29	−1.7	−2.9	109 ± 4	130 ± 4	−201 ± 4	−184 ± 4	−93 ± 5	−55 ± 5
3s5w24-6	Earth rotational slide	790	40	26	−0.4	−1.0	28 ± 5	70 ± 7	−64 ± 7	−184 ± 5	−36 ± 8	−115 ± 8
Average	—	2,952	35	29	−2.9	−3.0	—	—	—	—	—	—
Total	—	59,046	—	—	—	—	8,279 ± 42	11,138 ± 50	−26,391 ± 42	−22,851 ± 50	−18,112 ± 70	−11,713 ± 70

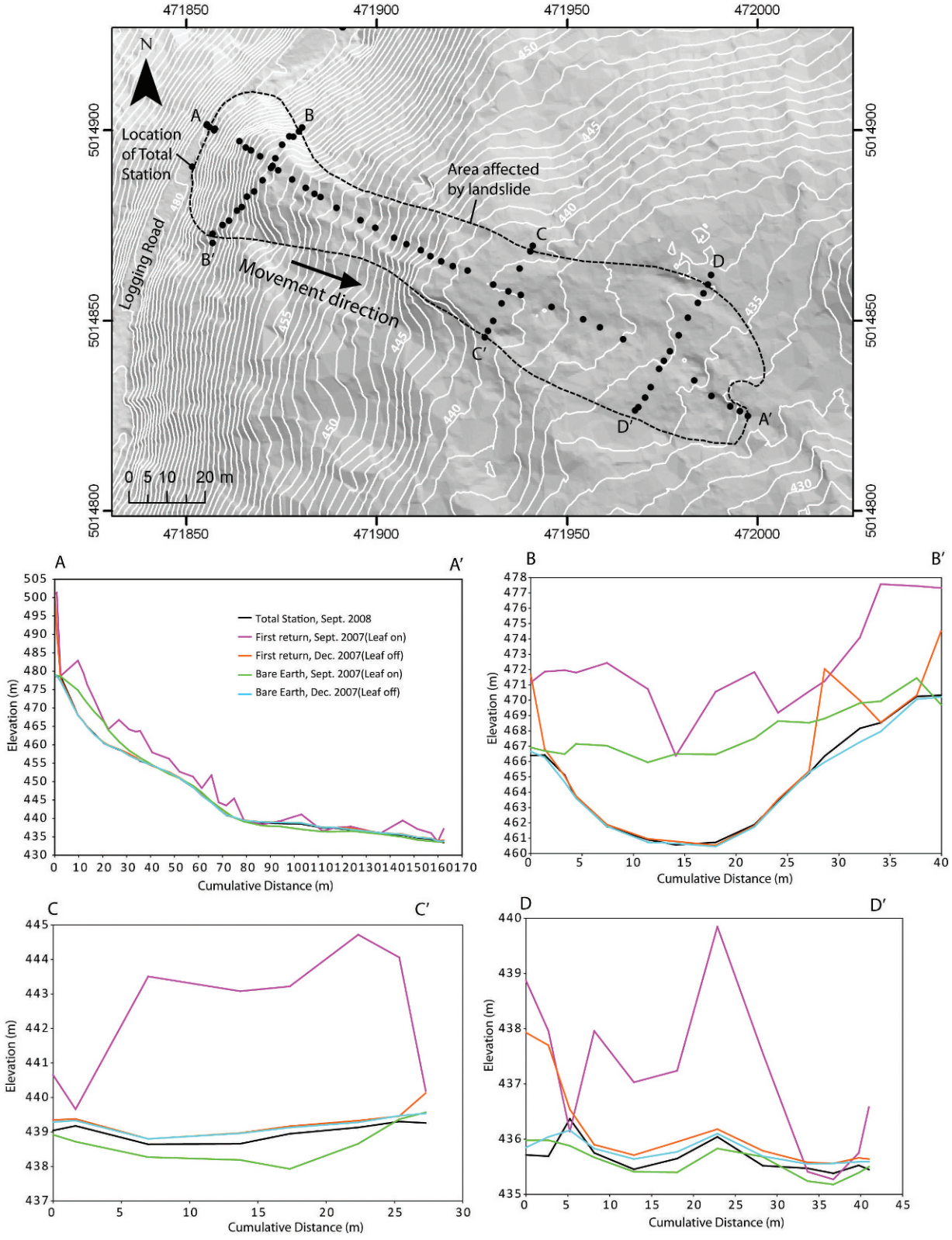

Figure 5. Plan view map and profiles of site 3s5w30-9. A photo of the site is given in Figure 9. UTM coordinates are shown on plan view map.

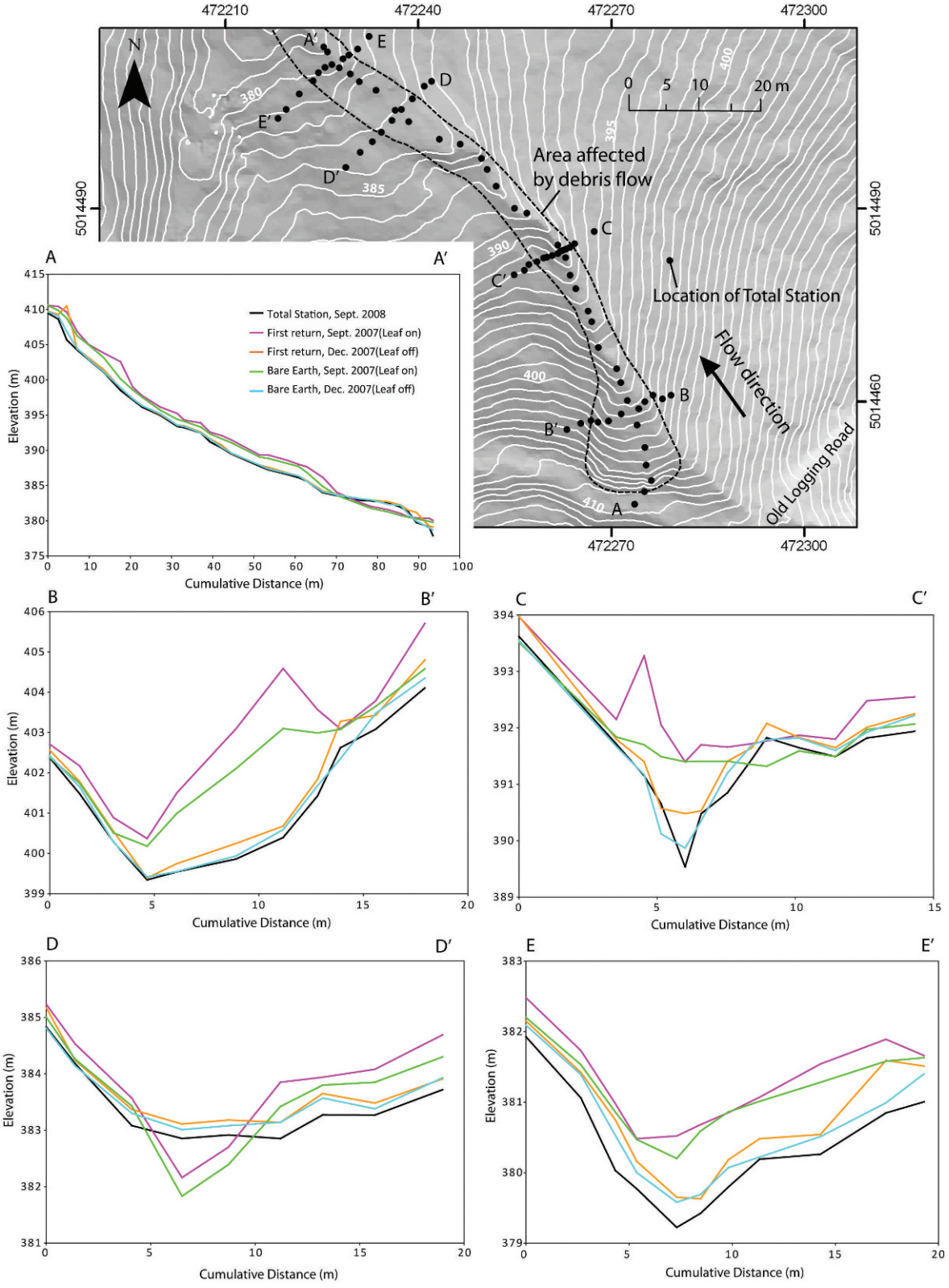

Figure 6. Plan view map and profiles of site 3s5w30-10. A photo of the site is given in Figure 10. UTM coordinates are shown on plan view map.

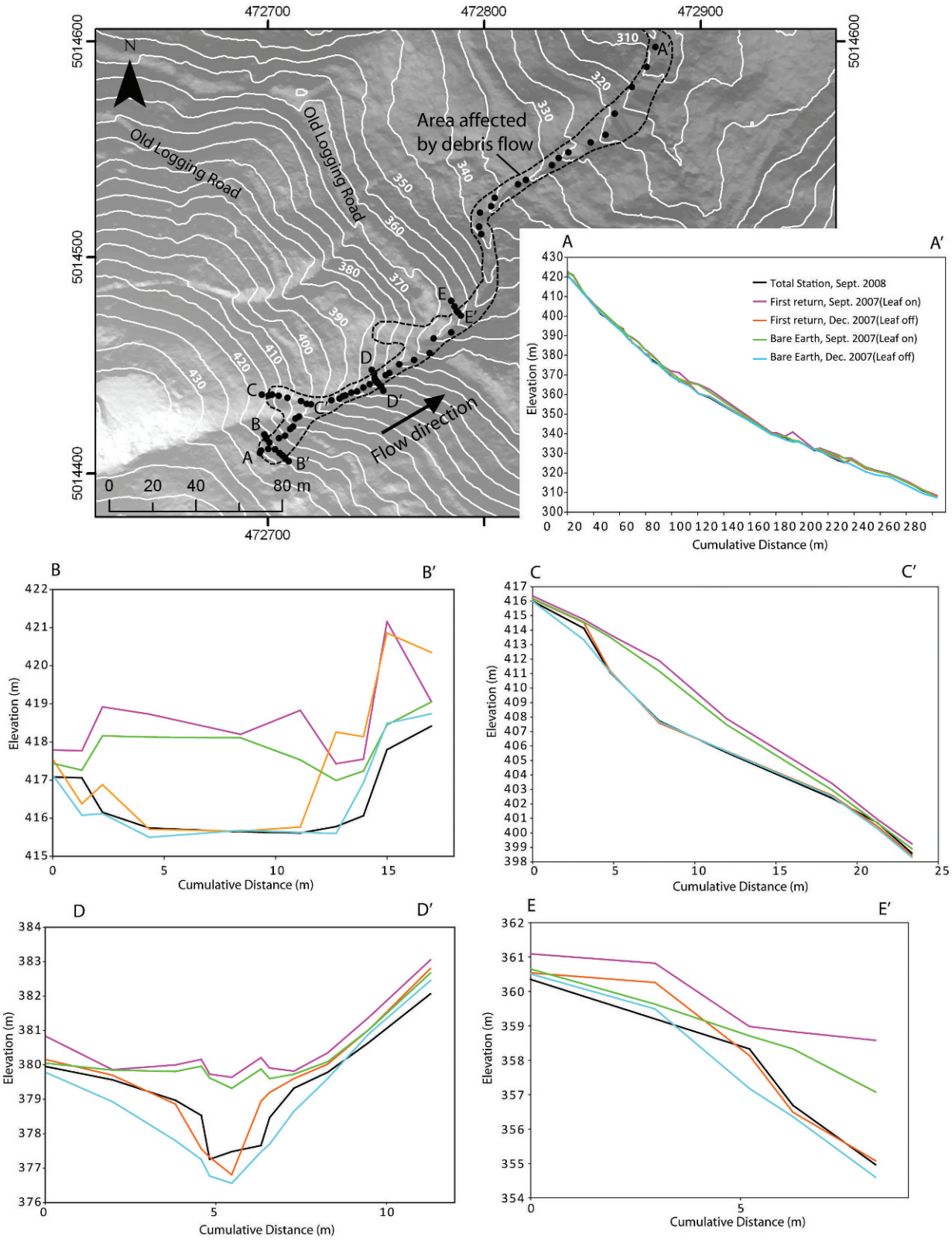

Figure 7. Plan view map and profiles of site 3s5w30-11. A photo of the site is given in Figure 11. UTM coordinates are shown on plan view map.

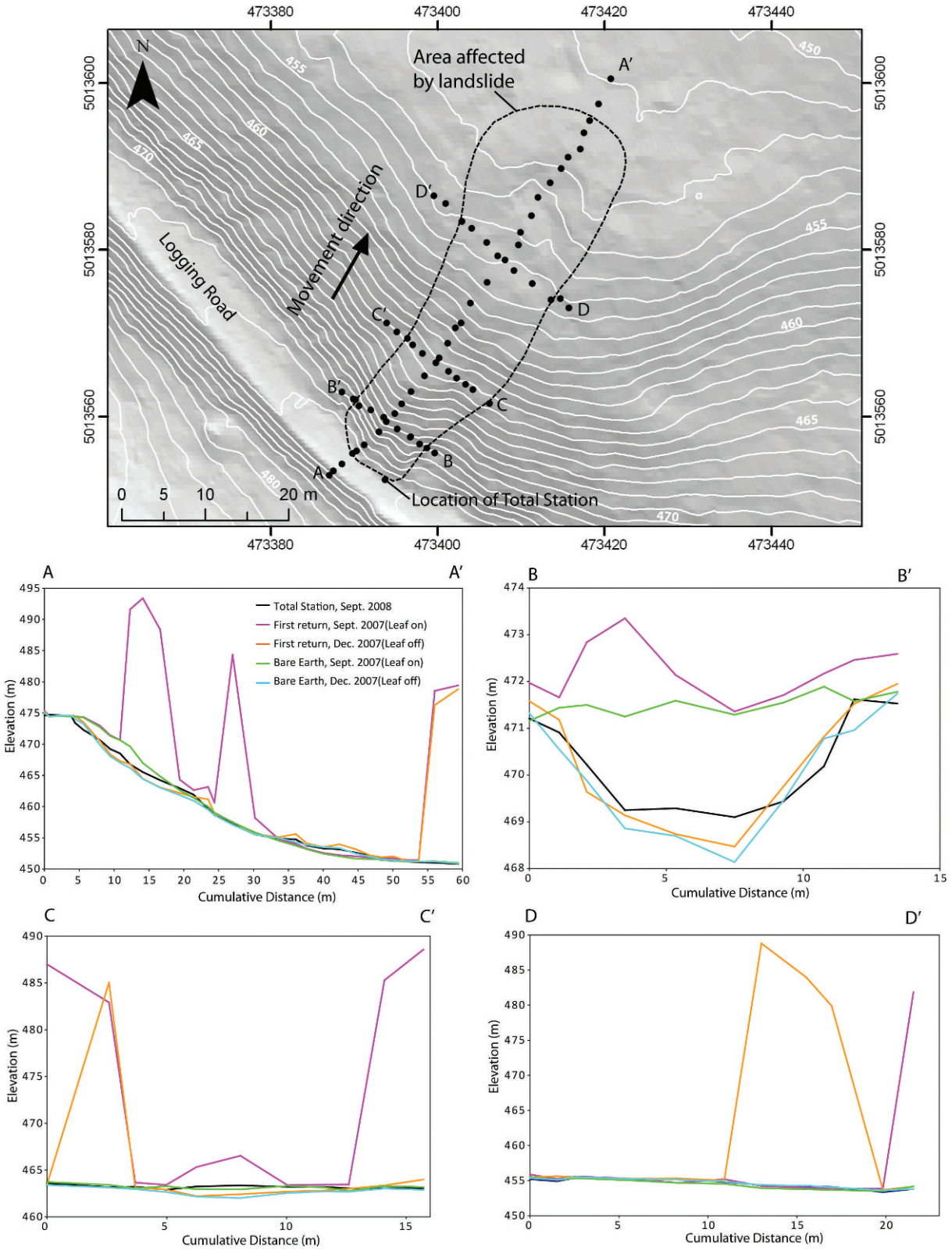

Figure 8. Plan view map and profiles of site 3s5w29-1. A photo of the site is given in Figure 12. A simple survey of this site was also done (see Table 2). UTM coordinates are shown on plan view map.

Table 4. *Comparison of elevations from total station data collected in September 2008 with bare-earth, leaf-off, Light Detection and Ranging (LiDAR) data from December 2007. See Figures 1, 5, 6, 7, and 8 for locations of sites and profiles. Negative maximum values and systematic errors (SEs) indicate that LiDAR data have higher elevations than do total station data. Positive maximum values and SEs indicate that LiDAR data have lower elevations than do total station data. Rows highlighted in bold text contain summary data for all profiles at individual sites or, in the case of the last row, all sites combined.*

Site No./Profile Name	No. of Measured Points	Maximum Error in Elevations (m)	Systematic Error in Elevations (m)	Root Mean Square Error in Elevations (m)	Comment(s)
3s5w30-9, A-A′	35	1.30	< −0.01	0.28	Maximum error at lip of retrogressing headscarp
3s5w30-9, B-B′	16	−0.90	−0.19	0.33	Maximum error on surface of internal (moving) slide block in source area
3s5w30-9, C-C′	8	0.30	0.20	0.21	Maximum error on landslide deposit
3s5w30-9, D-D′	12	0.35	0.11	0.17	Maximum error on landslide deposit
3s5w30-9, All profiles	**71**	**1.30**	**< −0.01**	**0.27**	**Maximum error at lip of retrogressing headscarp**
3s5w30-10, A-A′	31	−1.17	−0.20	0.33	Maximum error at base of steepest part of headscarp
3s5w30-10, B-B′	11	−0.39	−0.11	0.20	Maximum error on undisturbed ground on west side of source area
3s5w30-10, C-C′	13	0.53	−0.06	0.24	Maximum error at lip of incised channel
3s5w30-10, D-D′	9	−0.30	−0.15	0.19	Ground covered by thick, horsetail vegetation at point of maximum error
3s5w30-10, E-E′	11	−0.50	−0.27	0.30	Ground covered by thick, horsetail vegetation at point of maximum error
3s5w30-10, All profiles	**75**	**−1.17**	**−0.16**	**0.28**	**Maximum error at base of steepest part of headscarp**
3s5w30-11, A-A′	41	2.21	0.45	0.86	Maximum error at upper lip of incised, 2-m–deep channel
3s5w30-11, B-B′	10	0.98	−0.06	0.49	Maximum error at lip of lateral scarp in slide source area
3s5w30-11, C-C′	8	0.80	0.17	0.34	Maximum error at lip of headscarp
3s5w30-11, D-D′	12	1.28	0.49	0.70	Maximum error at upper lip of incised channel bank
3s5w30-11, E-E′	5	1.15	0.28	0.58	Maximum error on upper lip of channel bank failure
3s5w30-11, All profiles	**76**	**2.21**	**0.35**	**0.74**	**Maximum error at upper lip of incised, 2-m–deep channel**
3s5w29-1, A-A′	31	1.48	0.21	0.60	Maximum error in landslide source area
3s5w29-1, B-B′	10	0.96	0.23	0.48	Maximum error in landslide source area
3s5w29-1, C-C′	11	1.35	0.44	0.60	Maximum error on deposit of soil/ boulders
3s5w29-1, D-D′	11	−0.25	−0.08	0.13	Maximum error on undisturbed ground
3s5w29-1, All profiles	**63**	**1.48**	**0.21**	**0.53**	**Maximum error in landslide source area**
All sites, all profiles	**285**	**2.21**	**0.09**	**0.50**	**Maximum error at upper lip of incised, 2-m–deep channel**

elevation from the September 2008 total station survey was greater than the elevation from the December 2007 bare-earth LiDAR data. Therefore, we suspect that the error resulted from data processing to create the bare-earth model. Errors in the bare-earth DEMs are more common in very steep slope areas such as the headscarp area found at this landslide (e.g., McKenna et al., 2008).

The SE for all profile points at site 3s5w30-9 is <-0.01 m, which indicates that profile data from LiDAR have a very slight, systematic tendency to be at higher elevations than do data from the total station. Of the four individual profiles at the site, two have negative SEs and two have positive SEs (Table 4), but all are relatively small (less than 0.20 m). Based on field observations in September 2008, we strongly suspect that the SEs are small because there was very little to no vegetation present in the landslide area (Figure 9) in December 2007 when LiDAR data were acquired, and, therefore, minimal data processing was required to create the bare-earth DEM.

At site 3s5w30-10 (Figure 6), a landslide mobilized as a debris flow sometime between September 2007 and December 2007 (Figure 10). The landslide is located in a large clear-cut area and resulted from a

Figure 9. Photo of site 3s5w30-9. Plan and profile data are shown in Figure 5. Edge of road is visible in foreground. Note the young forest surrounding the deposit and the lack of any remaining vegetation in the landslide area.

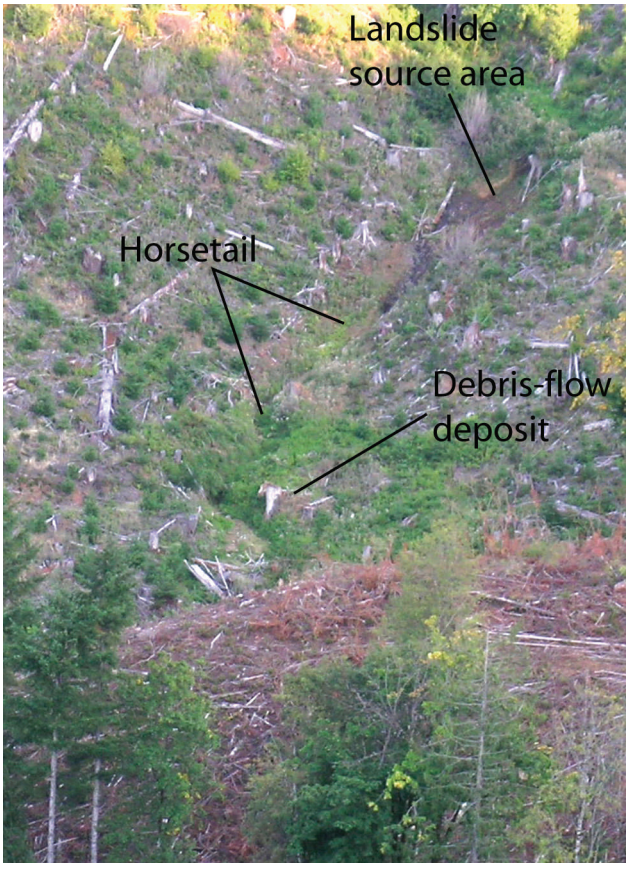

Figure 10. Photo of site 3s5w30-10. Plan and profile data of the site are shown in Figure 6.

failure of fill material underlying an abandoned logging road at a location where the road crosses a small drainage. When we visited the site in September 2008, multiple springs were present in the landslide source area. Elevation changes caused by the landslide and subsequent debris flow are visible when comparing profiles derived from bare-earth LiDAR data from September 2007 and December 2007 (Figure 6). Maximum elevation changes were about 3 m in the landslide source area (Figure 6, profiles A-A′ and B-B′) and about 1 m in the relatively flat debris-flow runout area (Figure 6, profile E-E′). The difference between bare-earth and first-return LiDAR data indicates that vegetation in the area prior to the landslide ranged up to about 2 m in height (Figure 6), which is in agreement with field observations of vegetation surrounding the site in September 2008 (Figure 10). A comparison of post-event, bare-earth LiDAR data from December 2007 and total station survey data from September 2008 indicate that the overall RMSE of bare-earth LiDAR data at the site is 0.28 m (site 3s5w30-10, All profiles; Table 4). RMSEs of individual profiles at the site range from 0.19 to 0.33 m. The maximum error (−1.17 m) is along profile A-A′ and is at the base of the steepest part of the landslide headscarp. The negative direction of the error indicates that the December 2007 LiDAR elevation was greater than the September 2008 total station elevation, a condition that could have been at least partly caused by post-event erosion. However, based on field observations and the magnitude and location of the error, we suspect that this negative error was most likely introduced by data processing to create the December 2007 LiDAR bare-earth DEM.

The SE for all profile points at site 3s5w30-10 is −0.16 m, which indicates that profile data from LiDAR have a systematic tendency to be at higher elevations than data from the total station. All four of the individual profiles at the site have negative SEs (Table 4). Based on field observations, we suspect that this SE was caused by the presence of thick giant horsetail (*Equisetum telmateia*) in the area (Figure 10) when the December 2007 LiDAR data were acquired. This type of vegetation tends to spread quickly into areas immediately after ground disturbance (such as a landslide) and tends to grow in wet soil areas.

At site 3s5w30-11 (Figure 7), debris flows were mobilized from two separate landslide source areas (one downslope from point A and the other down-

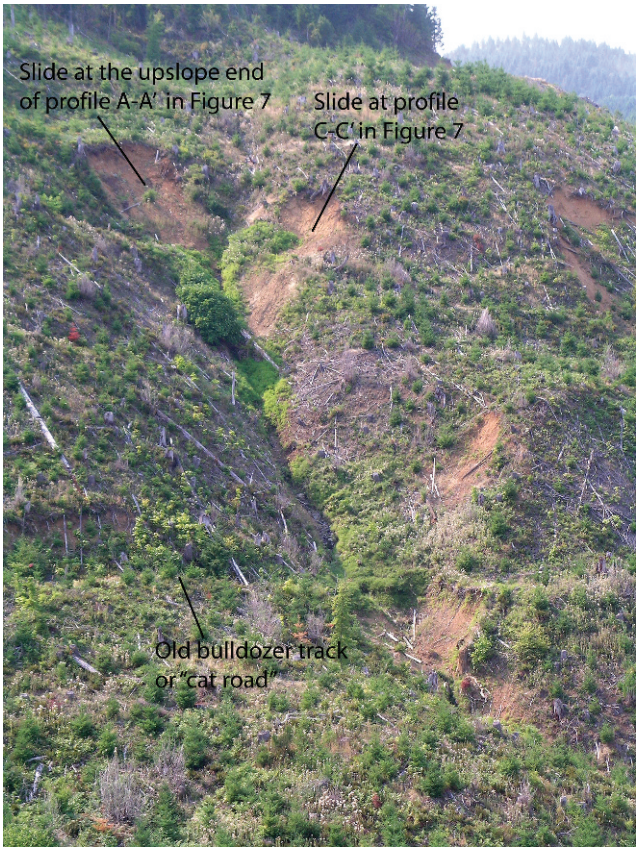

Figure 11. Photo of site 3s5w30-11. Plan and profile data of the site are shown in Figure 7.

slope from point C in Figure 7) between September 2007 and December 2007. Both landslides occurred on natural slopes in a clear-cut area (Figure 11). When we visited the site in September 2008, two small springs were present in the landslide source area downslope from point A, but none were observed in the area downslope from point C. Elevation changes caused by the landslides and subsequent debris flows are visible when comparing profiles derived from bare-earth LiDAR data from September 2007 and December 2007 (Figure 7). Maximum elevation changes were about 3 m in the landslide source areas (Figure 7, profiles A-A′, B-B′, and C-C′) and about 0.5 m in the relatively flat debris-flow deposition area near point A′. The difference between bare-earth and first-return LiDAR data indicates that vegetation in the area prior to the landslide ranged up to about 2 m in height (Figure 7, B-B′), which is in agreement with field observations of vegetation surrounding the site in September 2008 (Figure 11). A comparison of post-event, bare-earth LiDAR data from December 2007 and total station survey data from September 2008 indicates that the overall RMSE of bare-earth LiDAR data at the site is 0.74 m (site 3s5w30-11, All profiles; Table 4). RMSEs of individual profiles at the site range from 0.34 to 0.86 m. The maximum error (2.211 m) is along profile A-A′ and is at the upper lip of a narrow, deeply incised channel. The positive direction of the error indicates that the September 2008 total station elevation was greater than the December 2007 LiDAR elevation. From field observations, we know that the channel is about 2 to 3 m in depth and width and that the total station survey point was on the edge of the near-vertical channel wall. At this location, a small error (0.05 m or less) in the horizontal position of the LiDAR or total station data would result in a very large difference (in a positive direction) in the elevation value. We suspect that this situation is what caused the 2.2-m maximum error.

The SE for all profile points at site 3s5w30-11 is 0.35 m, which indicates that profile data from the LiDAR data have a systematic tendency to be at lower elevations than do data from the total station. Of the five individual profiles at the site, four have positive SEs, and one has a negative SE (Table 4). Because the channels were deeply incised and often covered by giant horsetail, many of our profile points were located along the upper slope break of the near-vertical channel wall. We suspect that the same situation that caused the maximum error (as described in the last paragraph) also caused the relatively large positive SE at the site. In support of this interpretation, the profile that had a negative SE (−0.06 m, B-B′) and the profile with the smallest positive SE (0.17 m, C-C′), were both located in landslide source areas, rather than along the incised channel.

At site 3s5w29-1 (Figure 8), a large landslide occurred between September 2007 and December 2007 (Figure 12). The landslide resulted from a failure of fill material underlying an active logging road through a partially thinned, forested area. A drainage culvert was present at the site and was visible in the landslide headscarp when we visited the site in September 2008. Additionally, we observed scattered large boulders (from a previous retaining wall) in the landslide scar and an older, more vegetated landslide deposit near the base of the slope. Both of these characteristics indicate that the site had been affected by a landslide prior to the late 2007 landslide. Elevation changes caused by the late 2007 landslide are visible when comparing profiles derived from bare-earth LiDAR data from September and December 2007 (Figure 8). Maximum elevation changes were about 3 m in the landslide source area (Figure 8, profile B-B′) and only a few decimeters in the relatively flat deposition area (Figure 8, profiles C-C′ and D-D′). First-return LiDAR data from the

Figure 12. Photo of site 3s5w29-1 taken looking upslope. Plan and profile data of the site are shown in Figure 8. Note boulders from previous retaining wall in the landslide scar, just below yellow total station at top of photo.

same two dates indicate that tree cover in the area prior to the landslide ranged up to 30 m in height (Figure 8). A comparison of post-landslide, bare-earth LiDAR data from December 2007 and total station survey data from September 2008 indicates that the overall RMSE of bare-earth LiDAR data at the site is 0.53 m (site 3s5w29-1, All profiles; Table 4). RMSEs of individual profiles at the site range from 0.13 to 0.60 m. The maximum error (1.48 m) is along profile A-A′ and is in the landslide source area. The error is positive, indicating that the elevation from the September 2008 total station survey was greater than the elevation from the December 2007 bare-earth LiDAR data. Based on field observations, we suspect that this error resulted from data processing to create the bare-earth DEM, rather than from actual elevation changes in the source area.

The SE for all profile points at site 3s5w29-1 is 0.21 m, which indicates that profile data from LiDAR have a systematic tendency to be at lower elevations than data from the total station. Of the four individual profiles at the site, one has a negative SE and three have positive SEs (Table 4). Based on field observations in September 2008, we suspect that these SEs resulted from data processing to create the bare-earth DEM, rather than from actual, post–December 2007 elevation changes.

DISCUSSION

Our map of primarily historical and prehistoric landslides includes 93 landslide deposits that cover about 28 percent of the study area (Figure 1). Previous small-scale (1:62,500) geologic mapping (performed roughly 15 years ago) resulted in the identification of seven large landslides, which comprised roughly 5 percent of the study area (Wells et al., 1994). The 0.5-m pixel resolution of the LiDAR data allowed us to map at a much larger scale (a maximum of about 1:2,000-scale) than the previous mapping effort and significantly improved our ability to identify large landslides in forested terrain. Additionally, we found that large landslides could be successfully identified and mapped from both leaf-off and leaf-on LiDAR data, although it was more difficult to accurately delineate landslide boundaries and scarps in the leaf-on data because of the presence of triangular facets where LiDAR point densities were low and elevations had been extensively interpolated for the creation of the bare-earth DEM.

Our analyses of two successive sets of LiDAR data (spaced 3 months apart) indicated that each individual LiDAR data set was very useful for mapping small to large ($\geq$384 m^2 of surface area) landslides, but that the difference in data set created by subtracting the first set of LiDAR data from the second set was less useful for detecting active landslides that occurred between the acquisition times of the two sets. Our analyses indicated that the detection of elevation changes due to active landslides could be improved through consistent acquisition of successive LiDAR data sets only during leaf-off seasons. Such acquisition would eliminate apparent elevation changes caused by differing levels of LiDAR penetration, point densities, and interpolation of elevations during processing to create a bare-earth DEM from successive leaf-on and leaf-off data sets (Figure 13). Compared to leaf-on conditions, leaf-off conditions increase LiDAR penetration and point densities and decrease the need for interpolation of elevations to create the bare-earth DEM. This was found to be especially true in areas with deciduous vegetation, young forest areas where short deciduous vegetation has the sunlight to grow, and/or areas with higher soil moisture (such as drainages), where conifer trees sometimes have a harder time growing and deciduous trees tend to thrive (Figure 13).

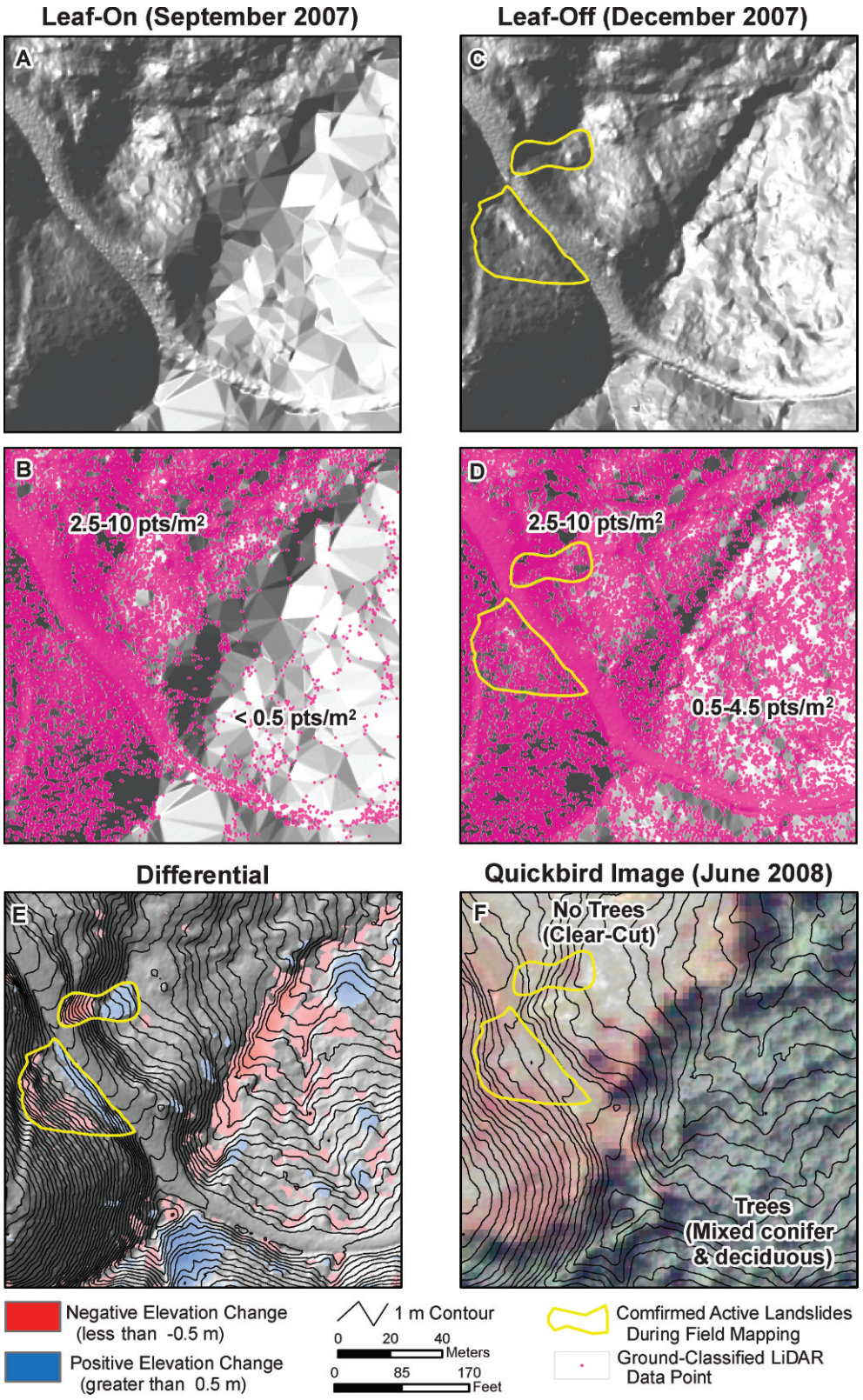

Figure 13. Maps of the change in the bare-earth DEM (A and C) derived from leaf-on data (B) and leaf-off data (D), respectively. The eastern portion of map A has the noticeable triangular faceted look as a result of the decrease in ground-classified points and the extensive interpolation of elevations between ground-classified points. Differential data (E) were derived by subtracting A from C. Note that the mixed conifer and deciduous trees in the drainage (F) that resulted in a significant reduction in ground-classified points.

From the differential LiDAR data set we were able to successfully identify and map active landslides, but to do so required the use of 1) thresholds (±0.50 m and ±0.75 m) to remove noise from the differential LiDAR data, 2) visual pattern recognition of areas of contiguous elevation changes and negative elevation changes in upslope areas and positive elevation changes in downslope areas, and 3) supplemental optical satellite imagery (QuickBird). After mapping, we field-verified 88 percent of landslides that we had mapped with high confidence, but we could not detect active landslides with elevation changes less than 0.50 m.

Our comparison of LiDAR elevations with elevations from simple surveys and total station surveys indicated that the most accurate LiDAR elevations were in areas that were clear-cut or had exposed bare ground from landslides when the LiDAR data were acquired. In these areas, our ground-based surveys indicate that the overall RMSE of elevations (in a single LiDAR data set) is about 0.5 m (Table 4). Within the study area, as well as in most forested areas in the Pacific Northwest, clear-cuts and areas of bare ground (sometimes found in mature forest areas) clearly represent the best ground conditions for acquiring the highest quality elevation data from airborne LiDAR.

In our study area, the RMSE of LiDAR elevations under vegetation cover was greater than 0.5 m. We make this inference on the basis of an observed increase of triangular facets in LiDAR data under vegetation, compared to a general lack of faceted areas in clear-cuts and bare-ground areas (Figure 13). Additionally, our two detailed survey sites that had the most vegetation (site 3s5w30-11, thick vegetation covering channels, Figure 11; and site 3s5w29-1, thin tree cover, Figure 12) had the highest overall RMSE values (0.74 m and 0.53 m, respectively) of the four sites surveyed.

The overall RMSE of the differential LiDAR data set (December 2007 minus September 2007 elevations) is 0.28 m. This RMSE is smaller than the RMSE from our comparison of the December 2007 LiDAR data to our ground-based survey points (i.e., 0.5 m). The relatively low RMSE of 0.28 m seems to indicate that airborne LiDAR data are able to produce relatively consistent elevation data in both leaf-on and leaf-off seasons. However, to further investigate the impact of leaf-on and leaf-off seasons on LiDAR quality, we evaluated both data sets in a representative area with active landslides, various types of vegetation cover, and a drainage channel (Figure 13). In Figure 13, the density of ground-classified LiDAR points is clearly greater during the leaf-off season than during the leaf-on season. For data acquired during the leaf-on season, the eastern portion of Figure 13 has a noticeable triangular faceted appearance, primarily due to the reduction of LiDAR ground-classified points in this area. The lack of ground-classified points is likely due to the blocking of the laser by relatively horizontal, broad leaves of deciduous trees. This decrease in ground-classified points results in an increase in the length of linear interpolation to create the TINs, resulting in poorer quality bare-earth DEMs.

Watershed Sciences (2008) reported that average ground-point densities in the study area decreased from 0.84 points/m^2 during the leaf-off season to 0.52 points/m^2 during the leaf-on season. In the area of Figure 13, the average ground-point density in the area of mixed conifers and deciduous vegetation during the leaf-on season was 0.15 points/m^2 (area mapped as $<$0.5 points/m^2), whereas during the leaf-off season, the average density of points in the same area is 1.1 points/m^2 (area mapped as 0.5 to 4.5 points/m^2). This difference in ground-point densities is particularly striking in the drainage channel (average leaf-on ground-point density just along the drainage channel is 0.06 points/m^2), where vegetation is thickest. This observation is in agreement with results from our ground-based survey data that showed that channels created problems for LiDAR because they often had steep walls and thick deciduous vegetation. In the channel in Figure 13, the difference in ground-point densities results in an extensive area of triangular facets where elevations have been interpolated. Thus, in the differential LiDAR data set, the channel area shows as an area of negative elevation change of up to 2.95 m that was verified in the field as completely false. Other portions of this channel area showed elevation changes that were positive, which were also false. These areas of false elevation change make it difficult to identify real areas of elevation changes caused by landslides (also shown in Figure 13) without fairly extensive fieldwork. This problem could be significantly improved if both data sets were flown in leaf-off seasons. In cases where leaf-off acquisition is not possible, it may be possible to increase the LiDAR pulse density (specifically, in areas of dense vegetation) so that ground-point densities are similar to those obtained during leaf-off seasons. An important qualifier to this statement is that, to our knowledge, no one has yet demonstrated that increasing pulse density during leaf-on seasons satisfactorily improves LiDAR penetration through dense vegetation.

The problem with low point densities during leaf-on season is reflected in the SE of the differential LiDAR DEM (−0.11 m) as well as in the calculated net volumes at active landslides sites (18 of 20 sites, or

90 percent, have negative net volumes; Table 3). The negative SE and negative volumes indicate that negative elevation changes outnumbered positive changes in the differential DEM. These negative changes were likely caused by lower elevations in the leaf-off DEM than in the leaf-on DEM or, said another way, by artificially high elevations in the leaf-on DEM. Three possible reasons for systematically lower elevations during leaf-off season are as follows. First, the lower elevations could be due to more LiDAR penetration to the ground surface during leaf-off season; second, the lower elevations could be caused by transport or erosion of loose, unvegetated landslide material out of the landslide areas into the active stream system and/or some contraction or compaction of material; or, third, the problem could be caused by an elevation indexing issue during data acquisition or post-processing. That is, elevations were indexed to a lower value in December 2007 than in September 2007. Our observations indicate that the systematically lower elevations were caused by the first and second reasons, that is, lower systematic elevations in the leaf-off DEM and removal of material by debris-flow transport and post-landslide erosion.

We found our RMSE value of 0.5 m (from our comparison of the December 2007 LiDAR data to our ground-based survey points) to be within the lower end of the range (from 0.16 to 3.26 m) found by previous assessments (discussed in the Introduction section of this article). We also found the overall RMSE of the differential LiDAR data set of 0.28 m to be within the lower end of this range (0.16 to 3.26 m). However, as was the case with previous studies, we found that the RMSE values can vary significantly within a study area with varying areas of steep slopes, heights and types of vegetation, and leaf conditions. In general, we concur with the previous studies that found an increase in RMSE values in areas with short, dense vegetation and/or deciduous tree cover (especially leaf-on conditions) and a decrease in RMSE values in areas of clear-cuts (or general lack of vegetation).

CONCLUSIONS

Results from this study lead us to make the following conclusions regarding the utility and limitations of LiDAR data in forested areas susceptible to landslides. Both leaf-on and leaf-off data can be used successfully to create inventories of historical and prehistoric deep-seated landslides. Our LiDAR-derived inventory map showed about 13 times more landslides than did previously mapped using conventional geologic mapping at a 1:62,500 scale.

Great care (caution) is needed when using differential DEMs created from multi-temporal LiDAR data to map, quantify, and interpret changes due to landslides, as well as other earth surface processes. Users of LiDAR data should not expect to simply subtract one LiDAR data set from another, at least in forested areas of the Pacific Northwest, to obtain a reliable differential DEM. We were able to successfully identify and map active landslides using a differential DEM, but to do so required the use of 1) thresholds (0.50 m and 0.75 m) to remove noise from the differential LiDAR data, 2) visual pattern recognition of areas of contiguous elevation changes and negative elevation changes in upslope areas and positive elevation changes in downslope areas, and 3) supplemental optical satellite imagery (QuickBird). After mapping, we field-verified 88 percent of landslides that we had mapped with high confidence, but we could not detect active landslides with elevation changes less than 0.50 m.

We were able to estimate volumetric changes caused by landslides, but, again, great care was needed when interpreting these changes. The impact of leaf-on/leaf-off conditions in the differential LiDAR DEM and actual changes caused by removal of material by transport and erosion must be taken into account when interpreting LiDAR-derived volumetric data.

For the optimum use of multi-temporal LiDAR data, all data sets should be flown during leaf-off seasons. In cases in which leaf-off acquisition is not possible, it may be possible to increase the LiDAR pulse density so that ground-point densities (in dense deciduous vegetation) are similar to those obtained during leaf-off seasons, but to our knowledge, this approach has not yet been successfully demonstrated. For the purposes of active landslide detection and mapping in the Pacific Northwest region of the United States, we recommend that multi-temporal LiDAR be collected during the early spring, before the majority of leaves have grown and right after the rainy season, when most landslides occur. Data acquisition during leaf-off seasons increases the density of LiDAR ground points used to interpolate bare-earth DEMS. In our study area, the most noticeable difference in the point densities between leaf-on and leaf-off seasons was in the mature forest and, especially, in young forest areas. Additionally, areas with mixed conifer-deciduous and deciduous types of vegetation displayed a noticeable decrease in ground-point densities in the LiDAR data acquired during the leaf-on season. This decrease in ground-classified point density conditions resulted in inaccurate elevations in the bare-earth DEM.

ACKNOWLEDGMENTS

We thank the Bureau of Land Management for providing the multi-temporal LiDAR data, QuickBird satellite imagery from June 2008, and other GIS data. The BLM also provided assistance in contacting the land owners in the Panther Creek Study area, which was very helpful. We would like to especially thank George McFadden and Susan Nelson from the BLM in Portland. We thank Ian Madin from DOGAMI, who had the initial idea to perform this study, and Jason Kean of the U.S. Geological Survey in Golden for his advice and assistance with the total station survey instrument. Permission was received from all land owners in the study area before the fieldwork was performed. We are grateful to Bill Haneberg, Jeffrey Keaton, Dennis Staley, Jon McKenna, and an anonymous reviewer for their thoughtful, constructive reviews of this article.

REFERENCES

Adams, J. and Chandler, J., 2002, Evaluation of LiDAR and medium-scale photogrammetry for detecting soft-cliff coastal change: *Photogrammetric Record*, Vol. 17, pp. 405–418.

Ardizzone, F.; Cardinali, M.; Galli, M.; and Reichenbach, P., 2007, Identification and mapping of recent rainfall-induced landslides using elevation data collected by airborne Lidar: *Natural Hazards Earth System Sciences*, Vol. 7, pp. 637–650.

Baltsavias, E. P., 1999, Airborne laser scanning: Basic relations and formulas: *Journal Photogrammetry Remote Sensing*, Vol. 54, pp. 199–214.

Baum, R. L.; Coe, J. A.; Godt, J. W.; Harp, E. L.; Reid, M. E.; Savage, W. Z.; Schulz, W. H.; Brien, D. L.; Chleborad, A. F.; McKenna, J. P.; and Michael, J. A., 2005, Regional landslide-hazard assessment for Seattle, Washington, USA: *Landslides*, Vol. 2, pp. 266–279.

Bowen, Z. H. and Waltermire, R. G., 2002, Evaluation of Light Detection and Ranging (LIDAR) for measuring river corridor topography: *Journal American Water Resources Association*, Vol. 38, No. 1, pp. 33–41.

Bureau of Land Management, 2005, *Forest Cover/Operations Inventory Publication Version GIS Database*: U.S. Department of the Interior, Bureau of Land Management, Tillamook, Oregon.

Bureau of Land Management and U.S. Forest Service, 1997, *Northern Coast Range Adaptive Management Area Guide*: Electronic document, available at http://www.fsl.orst.edu/ncama/guidcon.htm

Burns, W. J., 2007, Comparison of remote sensing datasets for the establishment of a landslide mapping protocol in Oregon. In Schaefer, V. R.; Schuster, R. L.; and Turner, A. K. (Editors), *Conference Presentations, 1st North American Landslide Conference, Vail, Colorado*: Association of Environmental & Engineering Geologists Special Publication 23, pp. 335–345.

Burns, W. J. and Madin, I. P., 2009, *Protocol for Inventory Mapping of Landslide Deposits from Light Detection and Ranging (lidar) Imagery*: Oregon Department of Geology and Mineral Industries, Special Paper 42.

Chen, R.; Chang, K.; Angelier, J.; Chan, Y.; Deffontaines, B.; Lee, C.; and Lin, M., 2006, Topographical changes revealed by high-resolution airborne LiDAR data: The 1999 Tsaoling landslide induced by the Chi-Chi earthquake: *Engineering Geology*, Vol. 88, pp. 160–172.

Coe, J. A.; Glancy, P. A.; and Whitney, J. W., 1997, Volumetric analysis and hydrologic characterization of a modern debris flow near Yucca Mountain, Nevada: *Geomorphology*, Vol. 20, pp. 11–28.

Corsini, A.; Borgatti, L.; Coren, F.; and Vellico, M., 2007, Use of multitemporal airborne lidar surveys to analyze post-failure behaviour of earth slides: *Canadian Journal Remote Sensing*, Vol. 33, pp. 116–120.

Dewitte, O.; Jasselette, J. C.; Cornet, Y.; Van Den Eeckhaut, M.; Collignon, A.; Poeses, J.; and Demoulin, A., 2008, Tracking landslide displacements by multi-temporal DTMs: A combined aerial stereogrammetric and LIDAR approach in western Belgium: *Engineering Geology*, Vol. 99, pp. 11–22.

Gatziolis, D. and Andersen, H. E., 2008, *A Guide to LIDAR Data Acquisition and Processing for the Forests of the Pacific Northwest*: U.S. Department of Agriculture, Forest Service, General Technical Report PNW-GTR-768, 32 p.

Glenn, N. F.; Streutker, D. R.; Chadwick, D. J.; Thackray, G. D.; and Dorsch, S. J., 2006, Analysis of LiDAR-derived topographic information for characterizing and differentiating landslide morphology and activity: *Geomorphology*, Vol. 73, pp. 131–148.

Hall, D. E.; Long, M. T.; and Remboldt, M. D. (Editors), 1994, *Slope Stability Reference Guide for National Forests in the United States, Forest Service Publication EM-7170-13*: U.S. Department of Agriculture, Washington, DC, United States Department of Agriculture, Vol. 2, pp. 331–343.

Haneberg, W. C., 2005, The ins and outs of airborne lidar—an introduction for practicing engineering geologists: *Association Engineering Geologists News*, Vol. 48, No. 1, pp. 16–19.

Haneberg, W. C., 2008, Elevation errors in a LiDAR digital elevation model of West Seattle and their effects on slope stability calculations. In Baum, R. L.; Godt, J. W.; and Highland, L. (Editors), *Landslides and Engineering Geology of the Greater Seattle Area, Washington: Geological Society of America Reviews in Engineering Geology*, Vol. 20, pp. 55–65.

Haneberg, W. C.; Creighton, A. L.; Medley, E. W.; and Jonas, D. A., 2005, Use of LiDAR to assess slope hazards at the Lihir gold mine, Papua New Guinea. In Hungr, O.; Fell, R.; Couture, R.; and Eberhardt, E. (Editors), *Landslide Risk Management: Proceedings of the International Conference on Landslide Risk Management*, Vancouver, Canada, 31 May–3 June, 2005, on Supplementary CD (not paginated).

Harding, D. J. and Berghoff, G. S., 2000, Fault scarp detection beneath dense vegetation cover: Airborne lidar mapping of the Seattle fault zone, Bainbridge Island, Washington State: *Proceedings American Society Photogrammetry and Remote Sensing Annual Conference*, Washington, DC, May 2000, 9 p.

Haugerud, R. A.; Harding, D. J.; Johnson, S. Y.; Harless, J. L.; Weaver, C. S.; and Sherrod, B. L., 2003, High-resolution Lidar topography of the Puget Lowland, Washington: *GSA Today*, Vol. 13, pp. 4–10.

Hodgson, M. E.; Jensen, J. R.; Schmidt, L.; Schill, S.; and Davis, B., 2003, An evaluation of LIDAR- and IFSAR-derived digital elevation models in leaf-on conditions with USGS Level 1 and Level 2 DEMs: *Remote Sensing Environment*, Vol. 84, pp. 295–308.

Hofmeister, R. J., 2000, *Slope Failures in Oregon: GIS Inventory for Three 1996/97 Storm Events*: Oregon Department of Geology and Mineral Industries Special Paper 34, 20 p.

Madin, I. P. and Burns, W. J., 2006, *Map of Landslide Geomorphology of Oregon City, Oregon and Vicinity Interpreted from LIDAR Imagery and Aerial Photographs*: Oregon

Department of Geology and Mineral Industries Open File Report O-06-27.

McKean, J. and Roering, J., 2004, Objective landslide detection and surface morphology mapping using high-resolution airborne laser altimetry: *Geomorphology*, Vol. 57, pp. 331–351.

McKenna, J. P.; Lidke, D. J.; and Coe, J. A., 2008, *Landslides Mapped from LIDAR, Kitsap County, Washington*: U.S. Geological Survey Open File Report 2008-1292, 81 p. Electronic document, available at http://pubs.usgs.gov/of/2008/1292/

National Climatic Data Center, 2008, *Haskins Dam, OR, Station, NOAA*: Electronic document, available at http://www4.ncdc.noaa.gov/cgi-win/wwcgi.dll?wwDI~StnSrch~StnID~20016321

Otte, G. E.; Setness, D. K.; Anderson, W. A.; Herbert, F. J.; and Knezevich, C. A., 1974, *Soil Survey of the Yamhill Area, Oregon*: U.S. Department of Agriculture, Soil Conservation Service, U.S. Government Printing Office, Washington, DC.

Reusser, L. and Bierman, P., 2007, Accuracy assessment of LiDAR-derived DEMs of bedrock river channels: Holtwood Gorge, Susquehanna River: *Geophysical Research Letters*, Vol. 34, p. L23S06, doi:10.1029/2007GL031329.

Reutebuch, S. E.; McGaughey, R. J.; Andersen, H.; and Carson, W. W., 2003, Accuracy of a high-resolution lidar terrain model under a conifer forest canopy: *Canadian Journal Remote Sensing*, Vol. 29, No. 5, pp. 527–535.

Roering, J. J.; Kirchner, J. W.; and Dietrich, W. E., 2005, Characterizing structural and lithologic controls on deep-seated landsliding: Implications for topographic relief and landscape evolution in the Oregon Coast range: *Geological Society America Bulletin*, Vol. 117, No. 5/6, pp. 654–668.

Scheidl, C.; Rickenmann, D.; and Chiari, M., 2008, The use of airborne LiDAR data for the analysis of debris flow events in Switzerland: *Natural Hazards Earth System Sciences*, Vol. 8, pp. 1113–1127.

Schulz, W. H., 2004, *Landslides Mapped from LIDAR Imagery, Seattle Washington*: U.S. Geological Survey Open-File Report 2004-1396, 11 p.

Schulz, W. H., 2007, Landslide susceptibility revealed by LIDAR imagery and historical records, Seattle, Washington: *Engineering Geology*, Vol. 89, pp. 67–87.

Slama, C. C.; Theurer, C.; and Henriksen, S. W., 1980, *Manual of Photogrammetry,* 4th ed.: American Society of Photogrammetry, Falls Church, VA, 1056 p.

Slatton, K. C.; Carter, W. E.; Shrestha, R. L.; and Dietrich, W., 2007, Airborne Laser Swath Mapping: Achieving the resolution and accuracy required for geosurficial research: *Geophysical Research Letters*, Vol. 34, L23S10, doi:10.1029/2007GL031939.

Soininen, A., 2004, *TerraScan User's Guide*: Terrasolid Ltd., Jyväskylä, Finland.

Staley, D. M.; Wasklewicz, T. A.; and Blaszczynski, J. S., 2006, Surficial patterns of debris flow deposition on alluvial fans in Death Valley, CA using airborne laser swath mapping data: *Geomorphology*, Vol. 74, pp. 152–163.

Varnes, D. J., 1978, Slope movement types and processes. In Schuster, R. L. and Krizek, R. J. (Editors), *Landslides Analysis and Control*: Transportation Research Board Special Report 176, pp. 11–33.

Watershed Sciences, Inc., 2008, *LiDAR Remote Sensing Data Collection*: Watershed Sciences, Inc., Yamhill County, OR, Unpublished document delivered with the lidar data.

Wehr, A. and Lohr, U., 1999, Airborne laser scanning—an introduction and overview: *Journal Photogrammetry Remore Sensing*, Vol. 54, pp. 68–82.

Wells, R. E.; Snavely, P. D.; MacLeod, N. S.; Kelly, M. M.; and Parker, M. J., 1994, *Geologic Map of the Tillamook Highlands, Northwestern Oregon Coast Range (Tillamook, Nehalem, Enright, Timber, Fairdale, and Blaine 15 minute Quadrangles)*: U.S. Geological Survey, Open File Report 94-21, 24 p.

White, S. A. and Wang, Y., 2003, Utilizing DEMs derived from LIDAR data to analyze morphologic change in the North Carolina coastline: *Remote Sensing Environment*, Vol. 85, pp. 39–47.

Woolard, J. W. and Colby, J. D., 2002, Spatial characterization, resolution, and volumetric change of coastal dunes using airborne LIDAR: Cape Hatteras, North Carolina: *Geomorphology*, Vol. 48, pp. 269–287.

Wooten, R. M.; Gillon, K. A.; Witt, A. C.; Latham, R. S.; Douglas, T. J.; Bauer, J. B.; Fuemmeler, S. J.; and Lee, L. G., 2008, Geologic, geomorphic, and meteorological aspects of debris flows triggered by Hurricanes Frances and Ivan during September 2004 in the southern Appalachian Mountains of Macon County, North Carolina (southeastern USA): *Landslides*, Vol. 5, pp. 31–44.